NASA TM X-767

TECHNICAL MEMORANDUM

X-767

COMPARISON OF EXPERIMENTAL CONTROL EFFECTIVENESS OF A FLAT-BOTTOM CANTED-NOSE HALF-CONE REENTRY CONFIGURATION WITH THAT OBTAINED BY SEVERAL METHODS OF PREDICTION FOR VARIOUS TYPES OF LOCAL FLOW AT A MACH NUMBER OF 6.0

By Paul F. Holloway

Langley Research Center
Langley Station, Hampton, Va.

NATIONAL AERONAUTICS AND SPACE ADMINISTRATION

WASHINGTON

March 1963

NATIONAL AERONAUTICS AND SPACE ADMINISTRATION

TECHNICAL MEMORANDUM X-767

COMPARISON OF EXPERIMENTAL CONTROL EFFECTIVENESS OF A FLAT-BOTTOM CANTED-NOSE HALF-CONE REENTRY CONFIGURATION WITH THAT OBTAINED BY SEVERAL METHODS OF PREDICTION FOR VARIOUS TYPES OF LOCAL FLOW AT A MACH NUMBER OF 6.0*

By Paul F. Holloway

SUMMARY

The experimental control effectiveness of the aerodynamic longitudinal and lateral controls (elevons) of a flat-bottom, canted-nose, half-cone reentry configuration (designated L-1 in NASA TM X-588) has been compared with that obtained by modified Newtonian predictions for both positive and negative control deflection angles, and for two control sizes so that the applicability of this theory for various local flow conditions could be determined. The experimental pressure distribution over the flat lifting surfaces, controls, and the side flat is presented for positive control deflection angles of 30° and 45° to determine the nature of the local flow and the effect of the control deflection on the loading distribution on the body. The tests were conducted over an angle-of-attack range of 0° to 60° at Reynolds numbers of 4.9×10^{6} to 6.6×10^{6} and at a Mach number of 6.0. Limited data are presented for Mach numbers of 3.18, 3.83, and 4.48.

It is shown that for a blunted, flat-bottom configuration of this type at hypersonic speeds the control effectiveness and the ability of modified Newtonian theory to predict this effectiveness is largely dependent upon the nature of the local flow over the bottom and control surfaces. Empirical relations are discussed for two types of local flow - supersonic separated flow over the control surface, and subsonic flow over both the bottom and control surfaces - for which modified Newtonian theory fails to give an accurate prediction of the experimental control effectiveness.

INTRODUCTION

There has been increasing interest in recent years in the use of lifting reentry vehicles for manned space flight missions such as earth orbital and circumlunar flights. It has been found in many previous studies (see refs. 1 to 4) that the use of lift during planetary entry results in increased corridor width

*Title, Unclassified.

for a given range of deceleration loads, a reduction in deceleration loads for a given entry angle, and the maneuverability necessary to reach a preselected landing site.

One method of modulating the lift of a reentry vehicle so that a preselected landing site may be reached is by the use of aerodynamic trailing-edge controls. The designer of such controls is faced with the problem of predicting the control effectiveness under many varied local flow conditions such as laminar, transitional, or turbulent boundary layers, attached or separated flow, and supersonic or subsonic local flow in the region of the control. There is to date no available theory that will give an accurate prediction of control effectiveness under these varying local flow conditions. However, one of the most widely used methods for preliminary prediction of control effectiveness at hypersonic Mach numbers is modified Newtonian theory.

It is the purpose of this paper to present the experimental control effectiveness of the aerodynamic controls (elevons) of a flat-bottom, canted-nose, half-cone reentry vehicle which was designated L-1 in reference 5. Aerodynamic characteristics of this configuration are presented in references 5 to 7. The control effectiveness is compared with that obtained by modified Newtonian predictions so that the applicability of this theory for various local flow conditions may be determined. In addition, two empirical methods of prediction based on the nature of the local flow are discussed. Experimental data include control effectiveness for both positive and negative deflections of the elevons determined by force tests and the local pressure distributions for the large positive control deflections (for which the local flow is most complex). The majority of the data presented is for a Mach number of 6.0. However, Mach number effect on control effectiveness is discussed for a Mach number range of 3 to 6 at comparable Reynolds numbers. Although the experimental results apply to a specific configuration, similar results would be expected for the more familiar blunted reentry bodies with flat bottoms and flat-plate-type controls such as delta-wing and wing-body configurations.

The tests were conducted over an angle-of-attack range of 0° to 60° at Reynolds numbers of 4.9×10^6 to 6.6×10^6 (based on the base diameter of the conical portion of the body) and at a Mach number of 6.0. Limited data are presented for Mach numbers of 3.18, 3.83, and 4.48.

SYMBOLS

ΔC_A incremental body axial-force coefficient, $\Delta F_A/q_\infty S$

ΔC_l incremental body rolling-moment coefficient, $\Delta M_X/q_\infty SD$

ΔC_m incremental body pitching-moment coefficient, $\Delta M_Y/q_\infty SD$

ΔC_N incremental body normal-force coefficient, $\Delta F_N/q_\infty S$

C_p	pressure coefficient based on free-stream conditions, $\frac{p_l - p_\infty}{q_\infty}$
ΔC_p	incremental pressure coefficient due to presence of deflected control
D	base diameter of conical portion of body, 2r
ΔF_A	incremental axial force due to deflection of controls from zero deflection angle
ΔF_N	incremental normal force due to deflection of controls from zero deflection angle
M	Mach number
ΔM_X	incremental rolling moment about assumed center of gravity due to differential deflection of controls
ΔM_Y	incremental pitching moment about assumed center of gravity due to deflection of controls from zero deflection angle
p_l	local static pressure
p_∞	free-stream static pressure
q_∞	free-stream dynamic pressure
R	Reynolds number based on base diameter of conical portion of body
r	base radius of conical portion of body (fig. 1)
S_e	control (elevon) reference
S_p	planform reference area (without controls)
s	surface distance along each ray (fig. 3)
X,Y,Z	body axes (fig. 1)
x,y,z	coordinates defining orifice location (fig. 3)
α	angle of attack measured from axis of cone
β	effective wedge angle
δ_a	aileron deflection angle defined as $\delta_{e,rt} - \delta_{e,lt}$
δ_e	control (elevon) deflection angle measured from axis of cone, positive for trailing edge down (fig. 1)
η	angle between velocity vector and a vector normal to body surface

Subscripts:

lt	left
rt	right

APPARATUS AND PROCEDURE

This investigation was conducted in the Langley 20-inch Mach 6 tunnel at Reynolds numbers from 4.9×10^6 to 6.6×10^6. The tunnel is of the blowdown-to-atmosphere type capable of operation to a maximum stagnation pressure of 580 lb/sq in. and a maximum stagnation temperature of 600° F. In addition, limited data at Mach numbers of 3.18, 3.83, and 4.48 obtained in the Langley 20-inch variable Mach number tunnel are presented. A description of the tunnels is given in reference 8.

A detailed drawing of the models (designated L-1 in ref. 5) is given in figure 1. All dimensions are given in terms of r, the base radius of the conical portion of the body. The models used for this investigation had a radius r of 3.84 inches.

Force Tests

The data of the force tests have been presented in reference 5.

The model support used for the force tests in the Mach 6.0 tunnel has its pitch plane horizontal and a pitch-angle range from -15° to 30°. In the variable Mach number tunnel, the pitch plane is vertical with a pitch-angle range of ±20°. The experimental data for angles of attack beyond this range were obtained by using stings bent in the pitch plane.

The elevons of the L-1 configuration have an area of 10 percent of the planform (reference) area. For the tests herein reported, data were also obtained with elevons having an area of 20 percent of the planform area for which the span was the same as that of the basic 10-percent elevons but the chord was doubled. The elevon deflection range investigated was from -50° to 45°.

A photograph showing a bottom view of the model and the various controls tested is shown as figure 2. For the results presented in this report, the rudder deflection was always 0°.

Pressure Tests

The instrumentation consisted of 31 pressure orifices located on one-half of the model only, since the configuration is symmetrical about the XZ-plane. Twenty-two orifices were located on the body and nine, on the control itself. The control deflections tested were 30° and 45° for both $S_e/S_p = 0.1$ and 0.2.

The rudders were not used during the pressure tests. Figure 3 shows the orifice locations with respect to rays on the body. The coordinates of each orifice, which lie along rays I, II, IV, and VI on the body and I_e, II_e, and III_e on the control, are given in table I. It should be noted that the model used for these tests was the same as that of reference 7; hence, the ray numbers of the orifice locations on the body are consistent with those of that reference. Ray I is located in the plane of symmetry of the body, and ray II, from the stagnation point (at 0° angle of attack) to the rear of the body at approximately one-half of the semispan of the flat lifting surfaces. There are circumferential rays at two stations along the axis of revolution of the cone, and three spanwise rays at three stations along the chord of the control. The surface distances along each ray are nondimensionalized by dividing by r.

The model support system for the pressure tests was the same as that of reference 7. The support system is designed to rotate through an angle-of-attack range of 90° in the vertical plane and to move vertically so that the model can be kept near the center of the tunnel.

The local static pressures on the body were recorded by photographing a multiple-tube manometer board using mercury as the fluid medium. Tunnel stagnation pressure was measured on a calibrated Bourdon gage.

Test Conditions

During the pressure tests it was necessary to increase the stagnation pressure as the angle of attack was increased so that the tunnel flow would remain established. The stagnation pressure for the force tests was 400 lb/sq in. giving a Reynolds number of 4.9×10^6 and, for the pressure tests, was varied from 450 to 535 lb/sq in. causing a variation in Reynolds number from 5.6×10^6 to 6.6×10^6.

Data Reduction

Previous tunnel flow calibrations have shown that the Mach number of the Mach 6.0 tunnel varies slowly as a function of time. This variation may range from $M = 6.02$ down to $M = 5.94$ and will cause a variation in the maximum pressure coefficient of about 7 percent. The Mach number variation across the tunnel test section at any given time has been found to be less than ± 0.02. Therefore, in the reduction of the data, a normal shock loss was assumed in the stagnation region, and the Mach number was then calculated from the maximum measured local pressure for each angle of attack by use of reference 9. This calculated Mach number was used to convert the measured local pressures to pressure coefficients.

RESULTS AND DISCUSSION

Local Flow Analysis

Schlieren photographs of the flow about the model are presented in figure 4. Figures 4(a) and 4(b) give the complete range of angle of attack in approximately 5° increments for the pressure tests with $\delta_e = 45^\circ$ and $S_e/S_p = 0.1$. Figure 4(c) shows the angle-of-attack range in approximately 10° increments for the pressure tests of the configuration with $\delta_e = 30^\circ$ and $S_e/S_p = 0.2$.

Inspection of figure 4(a) clearly shows the supersonic separation forward of the controls for the angles of attack up to 29°. Also, for $\alpha = 14^\circ$ to 29°, the overexpansion of the local subsonic flow from the blunt nose on to the bottom surface caused a separated region which is evident from the shock wave emanating from the reattachment point slightly rearward of the intersection of the two surfaces. (This phenomenon was also noted in ref. 7.) In figure 4(b), for angles of attack equal to or greater than 34°, the local flow field appears to be completely subsonic over the nose, bottom, and control surfaces. For $\alpha = 38.5^\circ$ and 42.5°, the compressed subsonic flow region between the bow shock wave and the locally separated region is accelerating, causing the formation of the normal shock wavelets similar to those found in reference 10.

In figure 4(c), for $\delta_e = 30^\circ$ and $S_e/S_p = 0.2$, the same flow patterns are noted, that is, supersonic separated flow for angles of attack up to 23.5° and an overexpansion region aft of the nose-bottom intersection for $\alpha = 13.5^\circ$ and 23.5°. Similarly, for $\alpha = 33.5^\circ$, the local flow is apparently subsonic, and for $\alpha = 41^\circ$, the normal wavelets are again apparent.

It is well known that the effectiveness of the controls depends on the nature of the local flow forward of the controls and over the control surface. For a free-stream Mach number of 6.0 on a blunted configuration of this type, the local flow may be supersonic or subsonic, as well as attached or separated depending upon the attitude of the configuration and the control deflection angle. If the flow is separated, the control effectiveness is further dependent upon the type of separation. Discussions of the characteristics of separated flows have been presented in many papers (for example, refs. 8 and 11 to 16). In particular, in reference 16, a brief discussion of the types of separation and the effect on the pressure distribution for these various types of separation is presented for a wedge on a flat plate. It is pointed out that, for subsonic separation, there is a maximum pressure occurring near the wedge leading edge which may reach the stagnation value. Also, a schematic drawing of laminar and turbulent types of separation is shown for supersonic local flow. Based on the known characteristics of the pressure distribution for turbulent separated flow and on the pressure data of this report (which is discussed in detail subsequently), the supersonic separation obtained in this investigation appeared to be always the turbulent type.

It is desirable to categorize the various local flow conditions of the tests considered herein for clarity of discussion. Thus, the flow conditions discussed are defined as follows (based on Newtonian pressure calculations with the assumption that the flow had previously passed through a normal shock):

supersonic attached flow: the local flow over both the bottom and control surfaces is supersonic and attached

subsonic flow: the flow over the bottom and control surfaces is completely subsonic ($\alpha > 38.5^\circ$; $\delta_e > 0^\circ$)

supersonic separated flow: the control deflection angle is large enough to cause separation and the flow is supersonic over the bottom surface and over the separated region ($(\alpha + \beta) < 38.5^\circ$)

mixed flow: the flow over the bottom surface is supersonic ($\alpha < 38.5^\circ$) and the flow over the control surface is subsonic ($(\alpha + \beta) > 38.5^\circ$)

In order to further clarify these conditions, figure 5 shows the effective wedge angle for the controls as a function of angle of attack. (The experimental data shown in this figure are from ref. 12.) This effective wedge angle is defined as the angle through which the local flow along the bottom surface must turn in passing over the control surface. The symbols represent the test points for the positive control deflection angles. (Note: $\beta = 0$ represents the bottom surface.) This figure is referred to in the discussion of the control effectiveness for positive deflection angles.

For all deflection angles the force and pressure data are compared with that obtained by modified Newtonian theory. ($C_p = C_{p,t} \cos^2\eta$, where $C_{p,t} = 1.818$, which is the stagnation pressure coefficient behind a normal shock for a Mach number of 6.0.)

Negative Control Deflections

Figures 6 and 7 show the experimental longitudinal control effectiveness (ΔC_m, ΔC_A, ΔC_N) for the negative elevon deflections compared with modified Newtonian theory. A comparison of theoretical predictions with experimental data shows that modified Newtonian theory predicts the control effectiveness very well for the case of supersonic attached local flow and for subsonic flow up to angles of attack of approximately 50°. For angles of attack of 50° and greater, the data begin to deviate slightly from the predictions for the -30° and -15° control deflections.

Positive Control Deflections - Attached Flow

In figure 8, the experimental longitudinal control effectiveness is compared with modified Newtonian predictions for a control deflection of 15° for which the effective wedge angle is 8° and the flow is theoretically attached. (The flow is theoretically supersonic and attached on the control surface up to an angle of attack of approximately 30°; see fig. 5.) A comparison of experimental data with theoretical predictions shows that, for supersonic attached flow over positively deflected controls, modified Newtonian theory predicts the control effectiveness reasonably well. As the flow becomes mixed, modified Newtonian predictions begin to deviate from experimental results, underpredicting the control effectiveness.

When the local flow becomes completely subsonic, modified Newtonian theory greatly underpredicts the control effectiveness with deviations of 100 percent of the predicted value of ΔC_N for both size controls.

Since the flow is supersonic and attached up to an angle of attack of approximately 30°, the control effectiveness is also compared with predictions based on oblique shock theory in figure 8. The comparison shows that shock theory better predicts the effectiveness of the controls than does modified Newtonian theory and, in particular, that it gives a more accurate prediction of the trends of the data.

An empirical method of prediction of control effectiveness based on the assumption of a parabolic pressure distribution over the bottom and control surfaces (see appendix) is presented in figure 8 for the condition of completely subsonic flow over these surfaces. Comparison of this method with experimental results shows that the assumed parabolic pressure distribution gives a much better prediction of the values of the control effectiveness and the trends of the data than does modified Newtonian theory.

It must be noted that this relation has been found to give a good prediction of control effectiveness and pressure distribution (as is discussed subsequently) for a specific configuration. It is possible, however, that this relation may predict these phenomena for other blunted, low-fineness-ratio configurations. Evidence to this end is presented in reference 16 where this relation is shown to give good agreement with the measured values of ΔC_N and the pressure distribution for a blunt-nose body with rectangular cross sections. This configuration is curved in the XZ-plane and the surface slope varies continually from the nose to the trailing edge of the body.

Positive Control Deflections - Separated Flow

Control effectiveness - force tests.- In figures 9 and 10, the experimental longitudinal control effectiveness is compared with modified Newtonian theory for $\delta_e = 30^\circ$ and 45° and $S_e/S_p = 0.1$ and 0.2 for which the local flow is theoretically supersonic and separated in the low angle-of-attack range (from fig. 5, up to $\alpha = 15.5^\circ$ for $\delta_e = 30^\circ$, and up to $\alpha = 0.5^\circ$ for $\delta_e = 45^\circ$). For the angle-of-attack range in which the local flow over the control surface is theoretically supersonic and separated, modified Newtonian theory overpredicts the control effectiveness. As the angle of attack is increased causing mixed flow over the bottom and control surfaces the experimental effectiveness increases up to and beyond the predicted value. When the angle of attack is increased beyond the point for which the local flow on the bottom and control surfaces is subsonic, modified Newtonian theory completely underpredicts control effectiveness. In the angle-of-attack ranges where mixed flow and subsonic flow occur, the deviation of theoretical predictions from experimental data is greater than 100 percent of the predicted value for ΔC_N, but generally is less than 50 percent of the predicted value for ΔC_m.

An empirical method of prediction of control effectiveness which was first presented in reference 16 is shown in figures 9 and 10 for the case of supersonic

turbulent separated flow over the control surface. For this method, a sinusoidal pressure distribution was assumed over the control surface from a maximum pressure (the peak pressure associated with turbulent separation for a forward-facing step) at the control leading edge to the Newtonian value at the trailing edge of the control. The peak pressure associated with a forward-facing step is a function of Mach number and was calculated from the equations of references 8 and 13. Comparison of the empirical sinusoidal pressure relation with modified Newtonian theory and the experimental data shows that the empirical method gives a better prediction of the control effectiveness for the supersonic separated region than does modified Newtonian theory.

For the subsonic flow range above $\alpha = 38.5^{\circ}$, the prediction of control effectiveness based on the empirical parabolic pressure distribution is compared with the experimental data and the theoretical predictions. For $\delta_e = 30^{\circ}$ and 45°, as well as for $\delta_e = 15^{\circ}$ (fig. 8), the empirical method gives a much better prediction of control effectiveness than does modified Newtonian theory and is particularly good in predicting the trend of the data.

Longitudinal pressure distributions.- In order to give a more detailed picture of the local flow phenomena for these large positive control deflections, figures 11 to 14 present the pressure distributions on the bottom and control surfaces.

Figure 11 gives the pressure distribution along rays I and II plotted against the nondimensionalized surface distance s/r. In figure 11(a), the pressure distribution over the basic body without aerodynamic controls is presented for basis of comparison (data taken from ref. 7). In figures 11(b) to 11(e), the pressure distribution over rays I and II is compared with modified Newtonian predictions for $\delta_e = 30^{\circ}$ and 45° and $S_e/S_p = 0.1$ and 0.2. In addition, the pressure distribution with controls deflected is compared with the distribution without aerodynamic controls. It should be noted that the data of point $s/r = 1.175$ on ray II appear low, indicating the possibility of a leaking tube.

In a comparison of modified Newtonian theory with the experimental data in figure 11, results similar to those of reference 7 are found. In particular, the midregions of the flat lifting surfaces are generally underpredicted. Modified Newtonian theory generally predicts the trend of the data although there is a large amount of local deviation between theory and experiment.

Comparison of the pressure distribution with controls deflected with that obtained on the basic configuration without aerodynamic controls gives a clearer understanding of the behavior of the control effectiveness. For supersonic separated flow over the control surface (see fig. 11), the local pressures on the controls are below the modified Newtonian predictions. Also, the measured pressures on the bottom surface forward of the controls are unaffected in the instrumented region. But as the flow becomes mixed and subsonic for increasing angles of attack, the pressures over the bottom surface are increased because of the presence of the controls. It has been noted that there is a much larger discrepancy between experimental data and theory for ΔC_N than for ΔC_m in figures 9 and 10. This result can be explained by inspection of the pressure distribution which shows that the control deflection causes a large increase in the loading distribution on the bottom surface forward of the controls. The result is a

large increase in normal force. However, this increased body loading distribution has small positive and negative moment arms relative to the center of gravity; consequently, the increase in pitching moment is relatively small compared with the increase in normal force. Similar results were also noted in reference 10 for a more generalized configuration - a flat delta wing with trailing-edge controls. The pressures on the nose of the L-1 configuration of this investigation are never affected by the control deflections for the angle-of-attack range investigated.

The empirical sinusoidal pressure distribution over the control surface is given for $\delta_e = 30^\circ$, $S_e/S_p = 0.1$ at $\alpha = 1.5^\circ$ and 11.5° and for $\delta_e = 30^\circ$, $S_e/S_p = 0.2$ at $\alpha = 3.5^\circ$ and 13.5° in figure 11. Values obtained by using the empirical relation agree reasonably well with the measured pressure distribution.

Incremental pressure distribution due to deflected controls.- Because this paper is concerned with control effectiveness, an examination should be made of the influence of the controls on the bottom surface pressures forward of the hinge line. In figure 12, the experimental incremental pressure is caused by the presence of the deflected controls for the case of local subsonic flow. This increase is compared with that in excess of the modified Newtonian value predicted by the empirical parabolic distribution of the appendix. Although, in figure 11, the parabolic distribution did not accurately predict the pressures measured on the bottom surface, figure 12 shows that this method does predict very well the actual increase in pressures along the bottom surface caused by the presence of the deflected controls. Also, it can be seen that as the local Mach number is decreased (α increasing), the agreement improves. It is interesting to note that based on figures 11 and 12, the increase in the chord of the elevon has no appreciable effect on the magnitude or location of the measured increase in pressures along the bottom surface.

Circumferential pressure distributions.- In order to show the effect of the control deflection on the circumferential pressure distribution around the body, figure 13 compares the experimental data for rays IV and VI with modified Newtonian theory and with the measured pressure distribution without aerodynamic controls. Again, the point on ray VI for $s/r = 0.325$ appears to be low, indicating a leaking tube. Modified Newtonian theory generally predicts the trends of the data and gives a good prediction of the distribution for the low angles of attack for which the local flow is supersonic.

Comparison of the pressure distributions for the controls deflected and for no controls in figure 13 shows that the pressures on the side cylinder and side flat are generally unaffected by control deflection and that the increase in pressure over the bottom surface due to the presence of the controls does not extend forward to ray VI except possibly for the angle-of-attack range where the flow is completely subsonic on the bottom and control surfaces.

Control pressure distributions.- Finally, figure 14 shows the spanwise pressure distribution along the three control rays for each deflection angle tested. Modified Newtonian theory generally overpredicts the pressures on the control surface due to separation when the local flow is supersonic and the strong pressure

relieving effects when the local flow is subsonic. The empirical sinusoidal pressure relation predicts the local pressures reasonably well where applicable.

The empirical parabolic pressure relation is very near the modified Newtonian predictions in magnitude for the control surface since for the range in which this relation is applicable the controls are nearly normal to the flow and these two methods of prediction are equivalent for a surface which is normal to the free-stream direction.

Roll Control Effectiveness

Roll control of the L-1 configuration is obtained by the differential deflection of the elevons. Therefore, it is desirable to see if the results of the comparison of modified Newtonian theory with the experimental control effectiveness in pitch are applicable to the case of roll control.

Figure 15 presents the roll control effectiveness compared with modified Newtonian predictions. As was found for the pitch control effectiveness, roll control effectiveness is overpredicted for supersonic (attached or separated) flow over the control surface. As the angle of attack is increased giving mixed or subsonic flow, modified Newtonian theory underpredicts the control effectiveness.

Mach Number Effect

Figure 16 presents the Mach number effects on pitch control effectiveness for a Reynolds number range of 4.9×10^6 to 10.7×10^6 and a Mach number range of 3 to 6. In general, the Mach number effects on control effectiveness are small for most deflection angles and angles of attack. The variation of control effectiveness that does occur is erratic, following no consistent scheme. This variation actually must be considered as a result of the variation of a variety of parameters including Mach number, Reynolds number, and their effect on the local boundary layer, and not thought of as a function of Mach number variation alone.

CONCLUDING REMARKS

The experimental control effectiveness of the aerodynamic longitudinal and lateral controls (elevons) of a flat-bottom, canted-nose, half-cone reentry vehicle (designated L-1 in NASA TM X-588) has been compared with that obtained by modified Newtonian predictions so that the applicability of this theory for various local flow conditions could be determined. The tests were conducted over an angle-of-attack range of 0° to 60° at Reynolds numbers of 4.9×10^6 to 6.6×10^6 at a Mach number of 6. Limited results are presented for Mach numbers of 3.18, 3.83, and 4.48.

It was found that modified Newtonian theory gives good agreement with experimental results when the flow over the bottom and control surfaces is completely supersonic and attached. However, if supersonic separation occurs over the control surface, modified Newtonian theory gives an overprediction of the control effectiveness. As the flow over the bottom and control surfaces becomes mixed (supersonic and subsonic) the theory begins to deviate from the experimental data, giving an underprediction of the data. The underprediction of the data increases as the subsonic region increases, with deviations of more than 100 percent of the predicted incremental body normal-force coefficient and almost 50 percent of the predicted incremental body pitching-moment coefficient for completely subsonic flow over the bottom and control surfaces.

For two types of local flow - supersonic separated flow, and subsonic flow - for which modified Newtonian theory fails to give an accurate prediction, it has been shown that empirical pressure distribution relations give a more accurate estimation of the measured control effectiveness and local pressure distribution.

Langley Research Center,
National Aeronautics and Space Administration,
Langley Station, Hampton, Va., December 10, 1962.

APPENDIX

METHOD OF PREDICTION OF CONTROL EFFECTIVENESS FOR LOCAL SUBSONIC FLOW

At large angles of attack and hypersonic flight speeds, flat-bottom configurations with trailing-edge controls such as the vehicle of this investigation may experience local subsonic flow over the bottom and control surfaces. Modified Newtonian theory cannot give an accurate prediction of the control effectiveness for such local flow conditions since it does not predict one very important phenomenon peculiar to flow conditions of this sort - the increase in pressure on the bottom surface caused by the presence of the deflected control in a subsonic stream.

In an effort to give a means of better predicting the loading distribution and control effectiveness for the condition of local subsonic flow over the bottom and control surfaces, a semiempirical relation was conceived based on the theoretical behavior of an incompressible fluid. In reference 16, a discussion of the nature of subsonic flow over a flat plate with a wedge points out that there is a maximum pressure occurring near the wedge leading edge which may reach the stagnation value. For an incompressible fluid flowing into a square corner, the velocity theoretically decreases linearly with distance to a value of zero at the corner junction. Hence, a linearly varying velocity would dictate that the pressure distribution vary parabolically.

For the empirical pressure distribution deduced from the known nature of subsonic flow and incompressible theory, modified Newtonian pressures are assumed at the trailing edge of the controls and at some point on the bottom surface. Parabolic pressure distributions (two dimensional) are then taken over both the bottom and control surfaces through a maximum pressure (stagnation) at the control leading edge.

The point at which the first effect on the pressures on the bottom surface is observed was assumed to be a function of the control deflection angle and the angle of attack given by

$$\frac{l}{L} = \frac{\delta}{(90^\circ - \alpha)}$$

where

l distance from control leading edge to beginning of parabolic pressure distribution on the bottom surface

L chordwise length of the flat-bottom surface

From this relation, the area on the bottom affected by the presence of the controls increases as both α and δ increase. Furthermore, the total bottom area is affected when the controls are normal to the free-stream direction for which $\alpha + \delta = 90^{\circ}$ (that is, $l/L = 1$). When $(\alpha + \delta) > 90^{\circ}$, that is, the controls are at some angle to the free-stream direction greater than 90°, the total bottom surface is considered affected and the equation is not necessary.

This method is restricted to positively deflected controls and angles of attack at least large enough to give subsonic flow over the bottom surface. In addition, the method does not apply if the controls extend through the body shock surface.

REFERENCES

1. Chapman, Dean R.: An Analysis of the Corridor and Guidance Requirements for Supercircular Entry Into Planetary Atmospheres. NASA TR R-55, 1960.

2. Becker, John V.: Re-Entry From Space. Scientific American, vol. 204, no. 1, Jan. 1961, pp. 49-57.

3. Lees, Lester, Hartwig, Frederic W., and Cohen, Clarence B.: Use of Aerodynamic Lift During Entry Into the Earth's Atmosphere. ARS Jour., vol. 29, no. 9, Sept. 1959, pp. 633-641.

4. Grant, Frederick C.: Importance of the Variation of Drag With Lift in Minimization of Satellite Entry Acceleration. NASA TN D-120, 1959.

5. Rainey, Robert W., compiler: Summary of Aerodynamic Characteristics of Low-Lift-Drag-Ratio Reentry Vehicles From Subsonic to Hypersonic Speeds. NASA TM X-588, 1961.

6. Armstrong, William O.: Aerodynamic Characteristics of a Flat-Bottom Canted-Nose Half-Cone Reentry Configuration at a Mach Number of 6.7. NASA TM X-630, 1962.

7. Holloway, Paul F.: Pressure Distribution on a Flat-Bottom Canted-Nose Half-Cone Reentry Configuration at a Mach Number of 6.0. NASA TM X-736, 1962.

8. Sterrett, James R., and Emery, James C.: Extension of Boundary-Layer-Separation Criteria to a Mach Number of 6.5 by Utilizing Flat Plates With Forward-Facing Steps. NASA TN D-618, 1960.

9. Ames Research Staff: Equations, Tables, and Charts for Compressible Flow. NACA Rep. 1135, 1953. (Supersedes NACA TN 1428.)

10. Fetterman, David E., and Neal, Luther, Jr.: An Analysis of the Delta-Wing Hypersonic Stability and Control Behavior at Angles of Attack Between 30° and 90°. NASA TN D-1602, 1963.

11. Chapman, Dean R., Kuehn, Donald M., and Larson, Howard K.: Investigation of Separated Flows in Supersonic and Subsonic Streams With Emphasis on the Effect of Transition. NACA Rep. 1356, 1958. (Supersedes NACA TN 3869.)

12. Kuehn, Donald M.: Experimental Investigation of the Pressure Rise Required for the Incipient Separation of Turbulent Boundary Layers in Two-Dimensional Supersonic Flow. NASA MEMO 1-21-59A, 1959.

13. Love, Eugene S.: Pressure Rise Associated With Shock-Induced Boundary-Layer Separation. NACA TN 3601, 1955.

14. Crocco, Luigi: Considerations of the Shock-Boundary Layer Interaction. Proc. Conf. on High-Speed Aeronautics, Antonio Ferri, Nicholas J. Hoff, and Paul A. Tilly, eds., Polytechnic Inst. of Brooklyn, c.1955, pp. 75-112.

15. Sterrett, James R., and Emery, James C.: Experimental Separation Studies for Two-Dimensional Wedges and Curved Surfaces at Mach Numbers of 4.8 to 6.2. NASA TN D-1014, 1962.

16. Staylor, W. Frank, Sterrett, James R., and Goldberg, Theodore J.: Pressure Distributions on a Blunt-Nose Lifting Reentry Body With Flaps at a Mach Number of 6.0 With Emphasis on the Nature of the Local Flow. NASA TM X-766, 1963.

TABLE I.- COORDINATES OF PRESSURE ORIFICES

Ray (a)	s/r	x, in.	y, in.	z, in.
Body orifices				
I	0.12	5.82	0	-1.44
	.29	5.37	.00	-.96
	.46	4.92	.00	-.48
	.56	4.65	.00	-.18
	.62	4.48	.00	-.08
	.69	4.23	.00	.00
	.86	3.58	.00	.11
	1.10	2.69	.00	.22
	1.33	1.79	.00	.33
	1.56	.90	.00	.44
Control orifices; $S_e/S_p = 0.1$; $\delta_e = 0^\circ$				
I	1.82	-0.10	0.30	0
	1.87	-.35	.30	.00
	1.93	-.50	.30	.00
Control orifices; $S_e/S_p = 0.2$; $\delta_e = 0^\circ$				
I	1.83	-0.15	0.30	0
	1.93	-.60	.30	.00
	2.04	-1.00	.30	.00
Body orifices				
II	0.70	4.48	1.14	-0.08
	.77	4.23	1.16	.00
	1.17	2.69	1.29	.22
	1.65	.90	1.44	.44
Control orifices; $S_e/S_p = 0.1$; $\delta_e = 0^\circ$				
II	1.90	-0.10	1.45	0
	1.96	-.35	1.45	.00
	2.01	-.50	1.45	.00
Control orifices; $S_e/S_p = 0.2$; $\delta_e = 0^\circ$				
II	1.92	-0.15	1.45	0
	2.03	-.60	1.45	.00
	2.12	-1.00	1.45	.00

Ray (a)	s/r	x, in.	y, in.	z, in.
Body orifices				
IV	0	0.90	0	0.44
	.37	.90	1.44	.44
	.75	.90	2.88	.44
	.81	.90	3.25	.34
	1.02	.90	3.39	-.40
	1.15	.90	3.48	-.90
VI	.00	2.69	.00	.22
	.33	2.69	1.29	.22
	.67	2.69	2.58	.22
	.73	2.69	2.93	.12
	.81	2.69	2.99	-.13
	.90	2.69	3.06	-.45
Control orifices; $S_e/S_p = 0.1$; $\delta_e = 0^\circ$				
I_e	0.08	-0.10	0.30	0
	.38	-.10	1.45	.00
	.68	-.10	2.60	.00
Control orifices; $S_e/S_p = 0.2$; $\delta_e = 0^\circ$				
I_e	0.08	-0.15	0.30	0
	.38	-.15	1.45	.00
	.68	-.15	2.60	.00
Control orifices; $S_e/S_p = 0.1$; $\delta_e = 0^\circ$				
II_e	0.08	-0.35	0.30	0
	.38	-.35	1.45	.00
	.68	-.35	2.60	.00
Control orifices; $S_e/S_p = 0.2$; $\delta_e = 0^\circ$				
II_e	0.08	-0.60	0.30	0
	.38	-.60	1.45	.00
	.68	-.60	2.60	.00
Control orifices; $S_e/S_p = 0.1$; $\delta_e = 0^\circ$				
III_e	0.08	-0.50	0.30	0
	.38	-.50	1.45	.00
	.68	-.50	2.60	.00
Control orifices; $S_e/S_p = 0.2$; $\delta_e = 0^\circ$				
III_e	0.08	-1.00	0.30	0
	.38	-1.00	1.45	.00
	.68	-1.00	2.60	.00

[a]Locations of rays shown in figure 3.

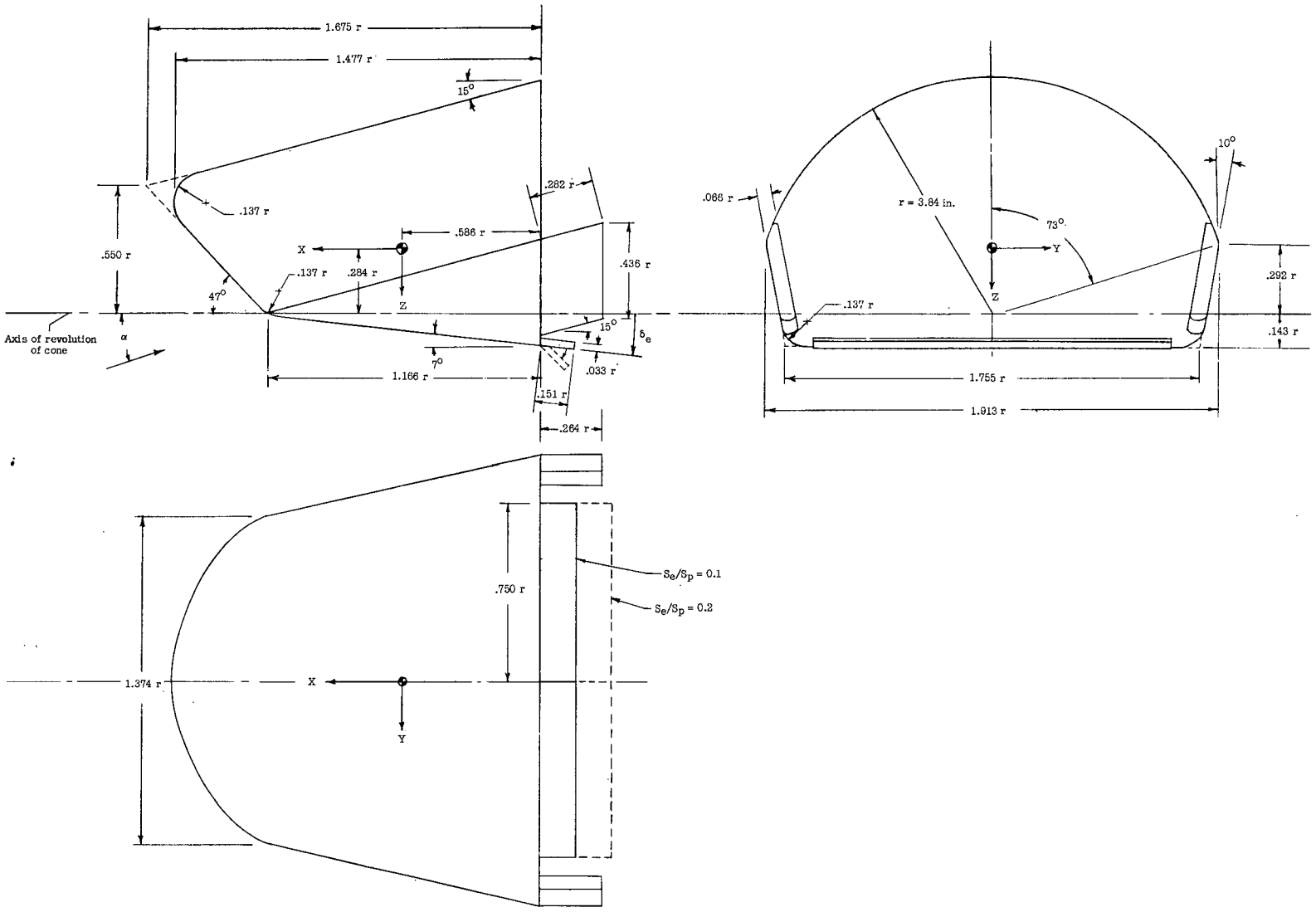

Figure 1.- L-1 configuration and dimensions.

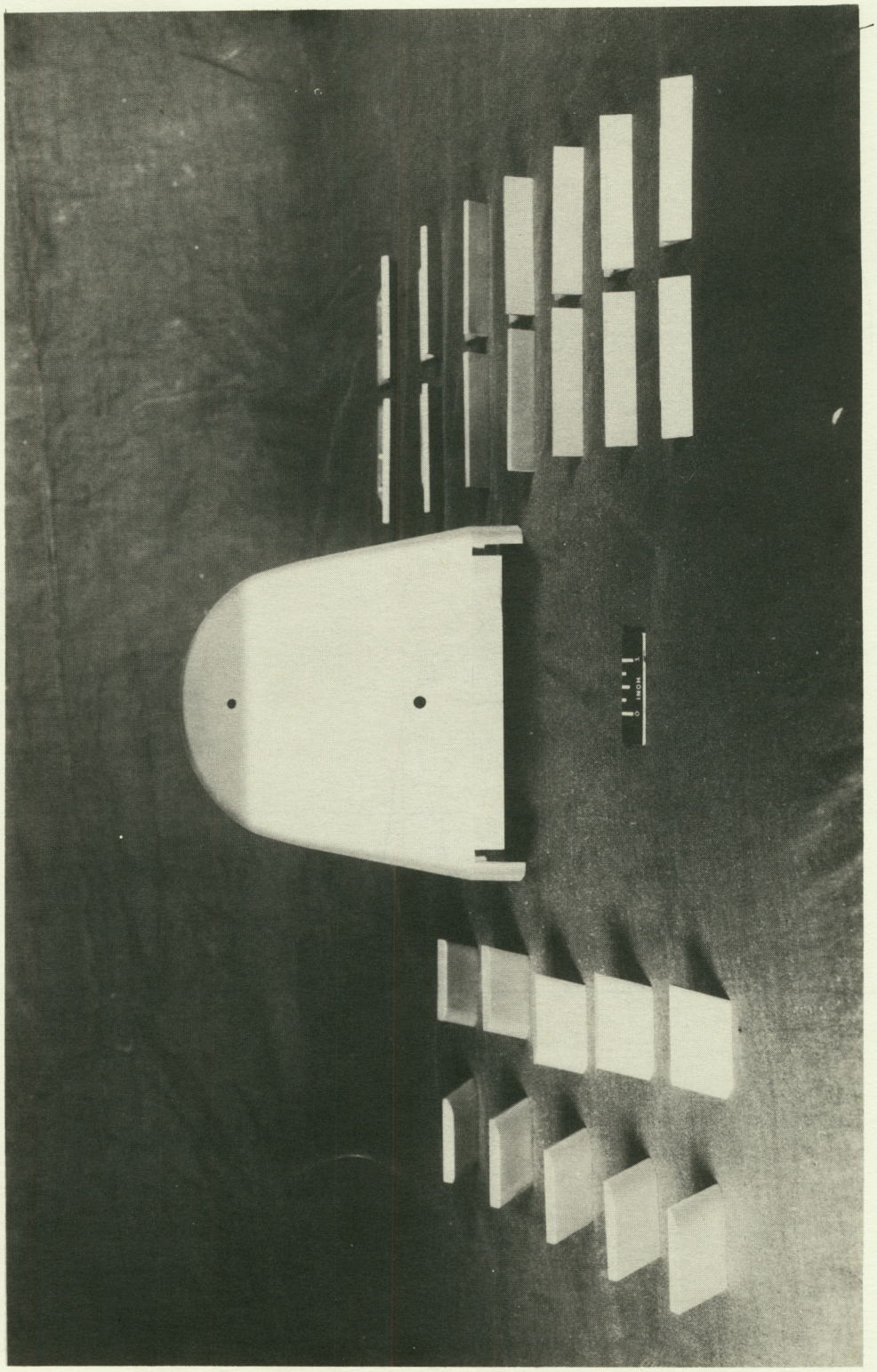

Figure 2.- Photograph showing bottom view of L-1 model and the controls tested. L-60-7088

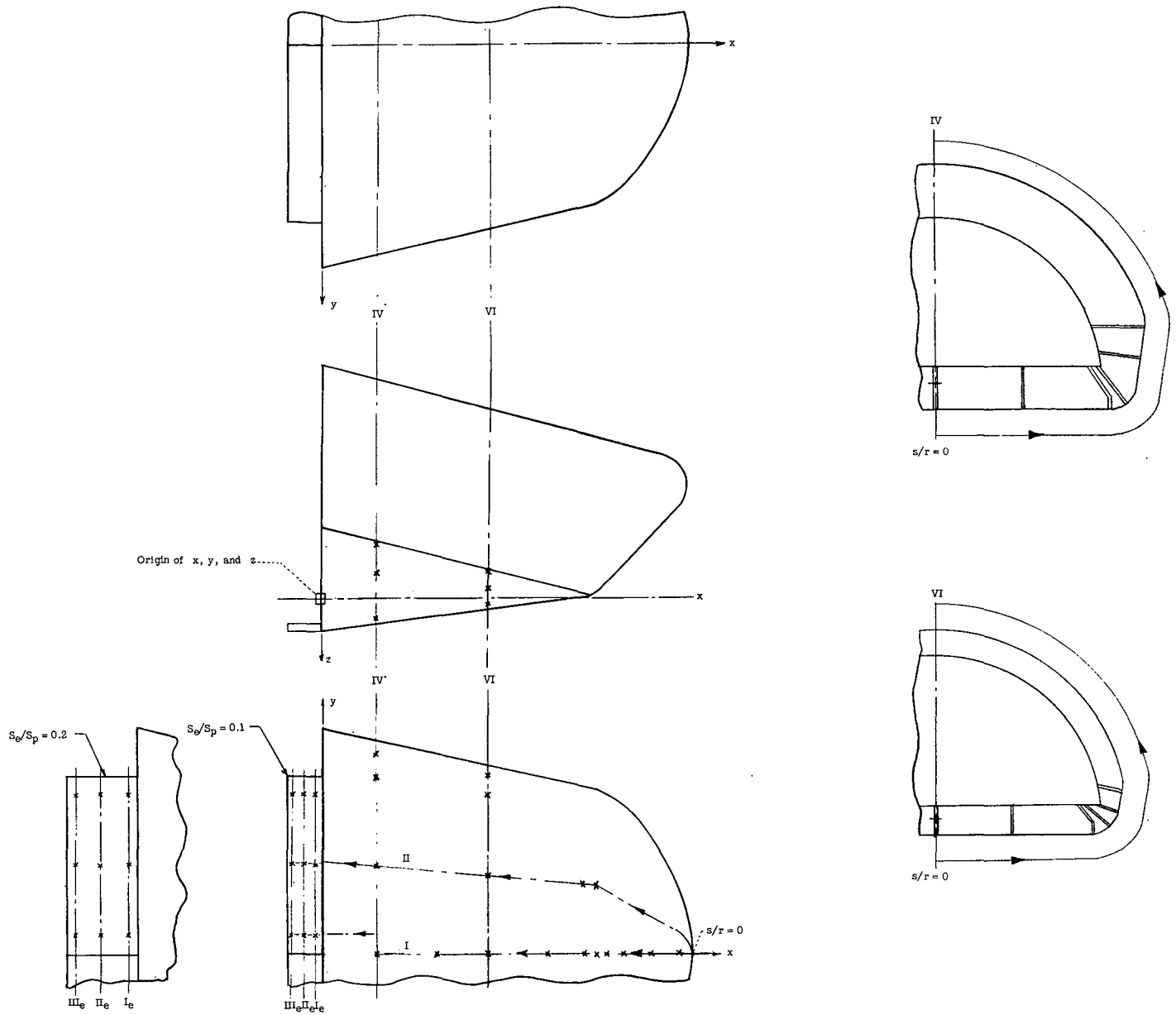

Figure 3.- Schematic location of pressure orifices.

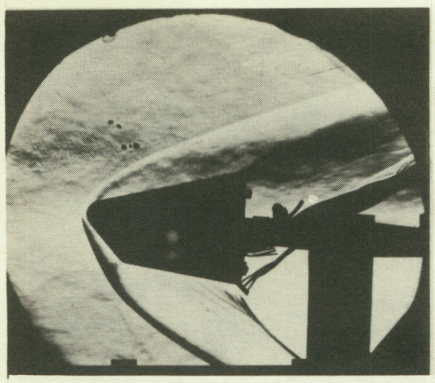

$\alpha = 4^{\circ}$

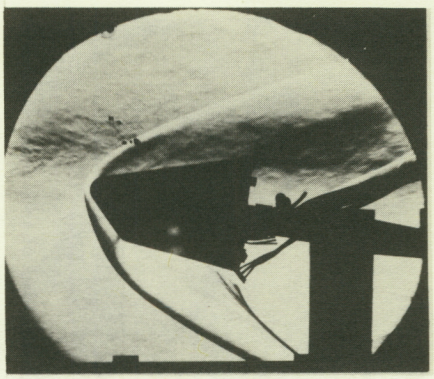

$\alpha = 9^{\circ}$

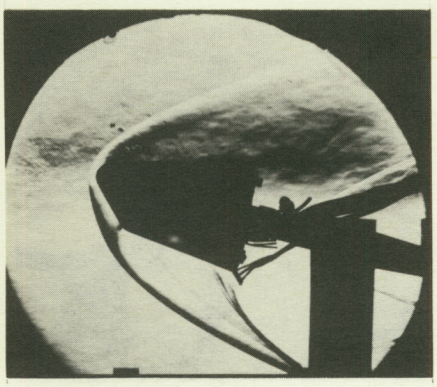

$\alpha = 14^{\circ}$

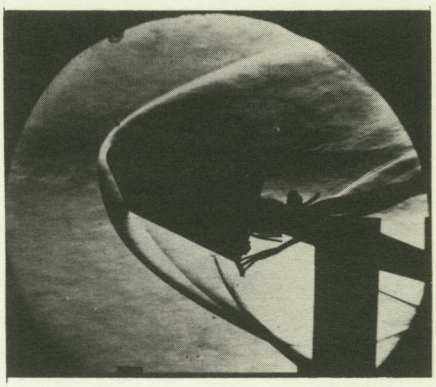

$\alpha = 18.5^{\circ}$

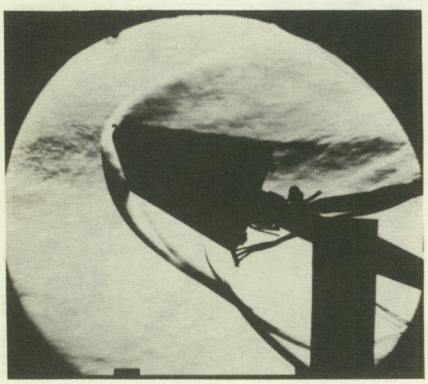

$\alpha = 23.5^{\circ}$

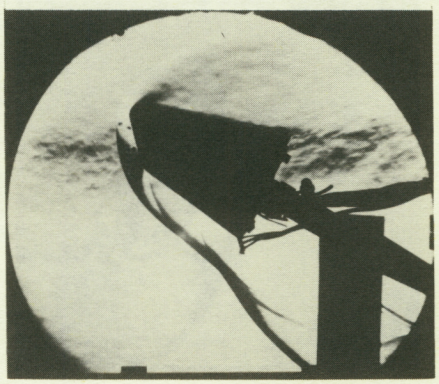

$\alpha = 29^{\circ}$

(a) $\delta_e = 45^{\circ}$; $S_e/S_p = 0.1$; $\alpha = 4^{\circ}$ to 29°. L-62-7060

Figure 4.- Schlieren photographs taken during pressure tests for two control deflections at various angles of attack.

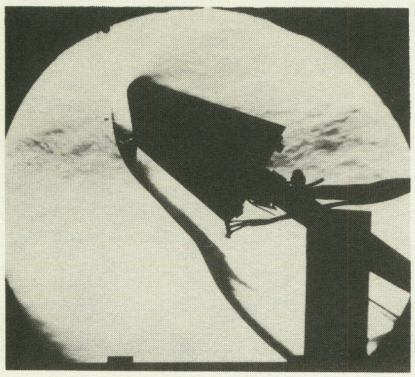

$\alpha = 34^{\circ}$

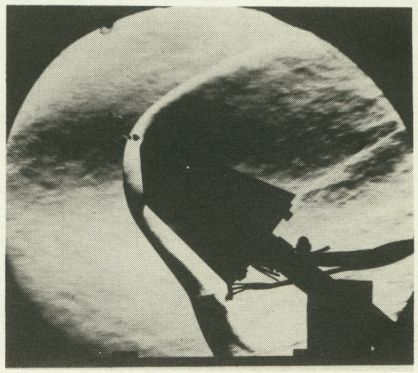

$\alpha = 38.5^{\circ}$

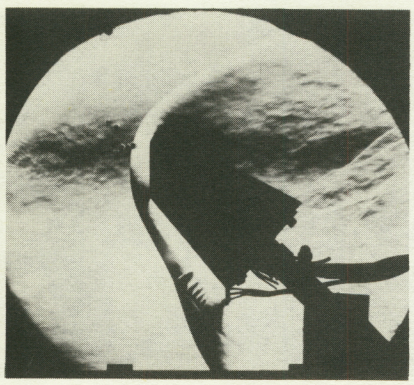

$\alpha = 42.5^{\circ}$

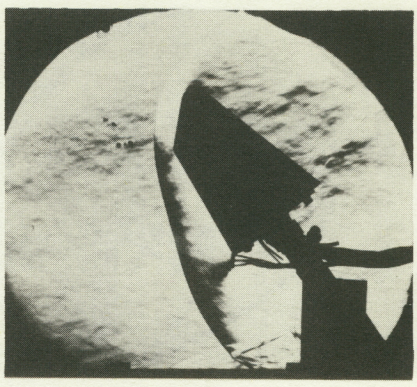

$\alpha = 52.5^{\circ}$

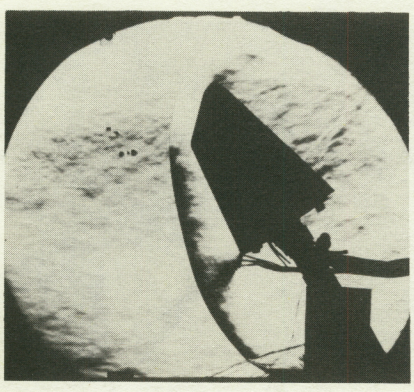

$\alpha = 58^{\circ}$

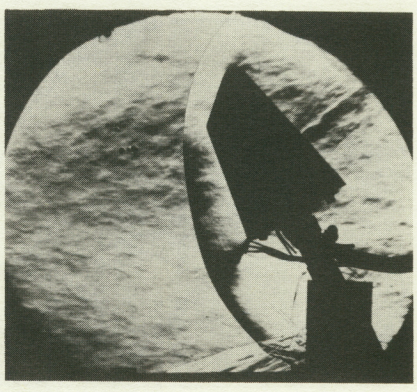

$\alpha = 63^{\circ}$

(b) $\delta_e = 45^{\circ}$; $S_e/S_p = 0.1$; $\alpha = 34^{\circ}$ to 63°. L-62-7061

Figure 4.- Continued.

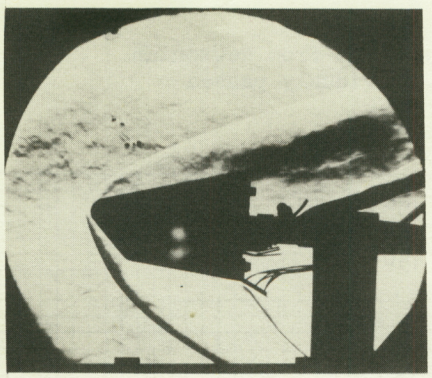

$\alpha = 3.5^{\circ}$

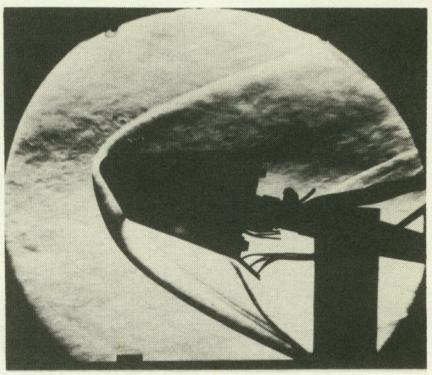

$\alpha = 13.5^{\circ}$

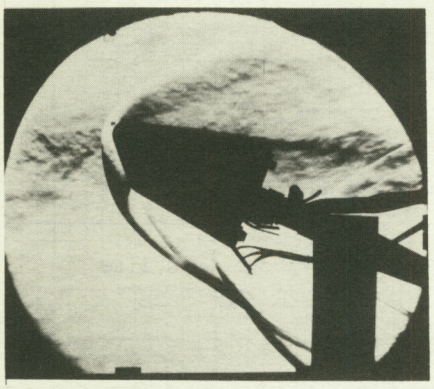

$\alpha = 23.5^{\circ}$

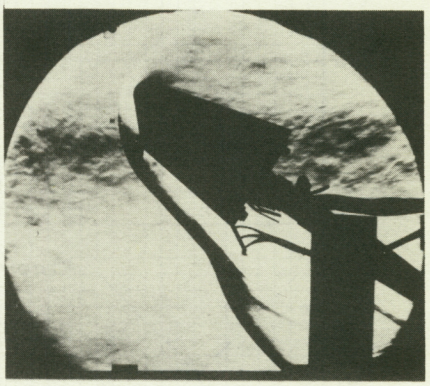

$\alpha = 33.5^{\circ}$

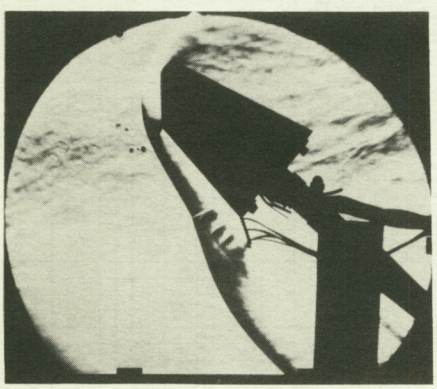

$\alpha = 41^{\circ}$

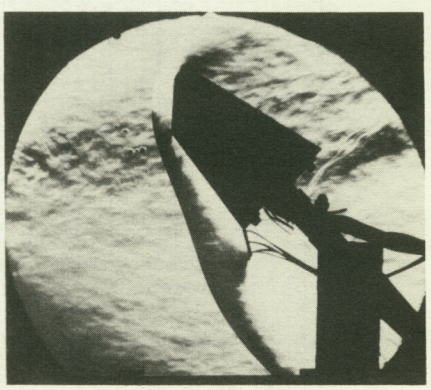

$\alpha = 47.5^{\circ}$

(c) $\delta_e = 30^{\circ}$; $S_e/S_p = 0.2$; $\alpha = 3.5^{\circ}$ to 47.5°. L-62-7062

Figure 4.- Concluded.

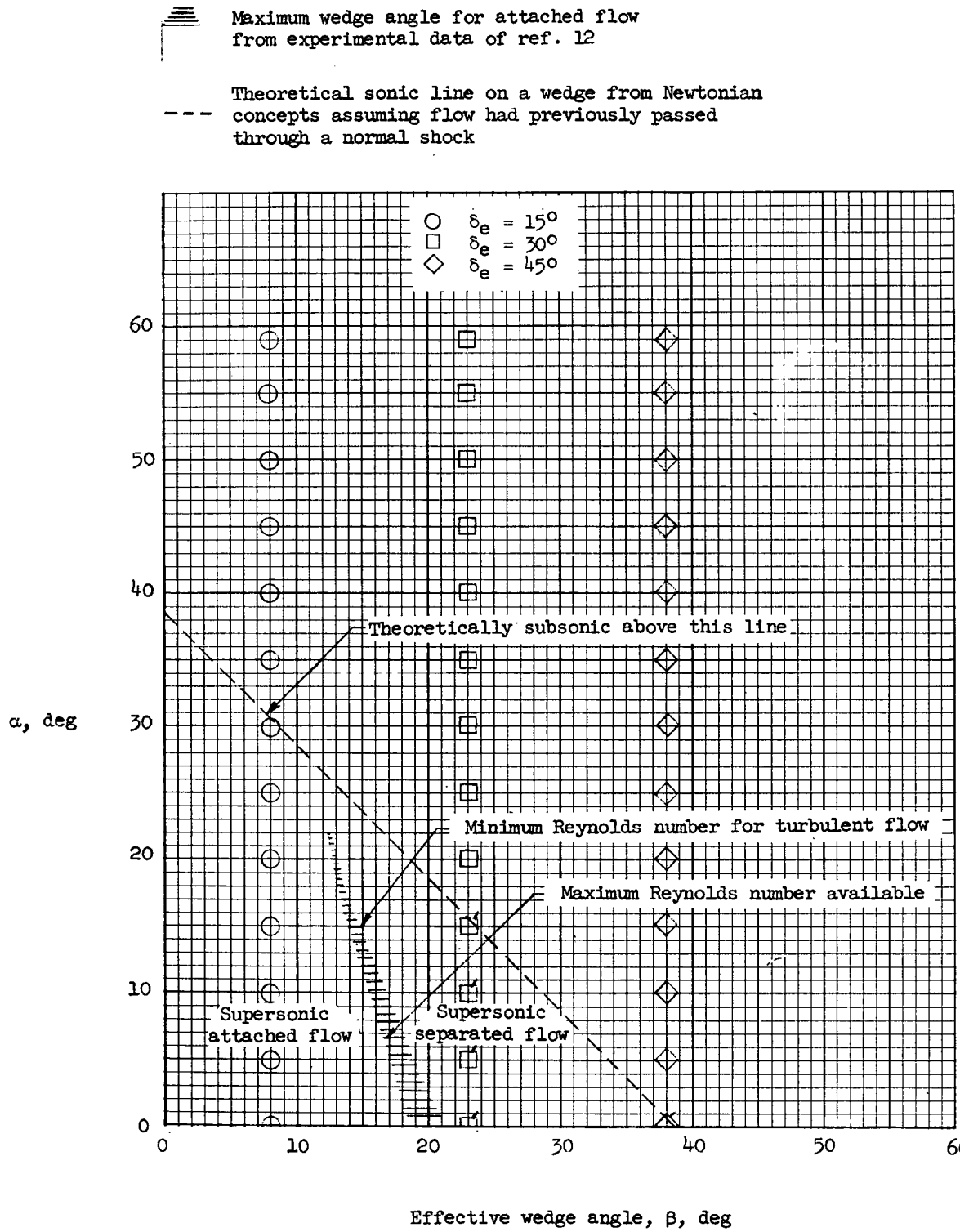

Figure 5.- Effective wedge angle for controls as a function of angle of attack. Flagged symbols are for experimental flows with a separated region.

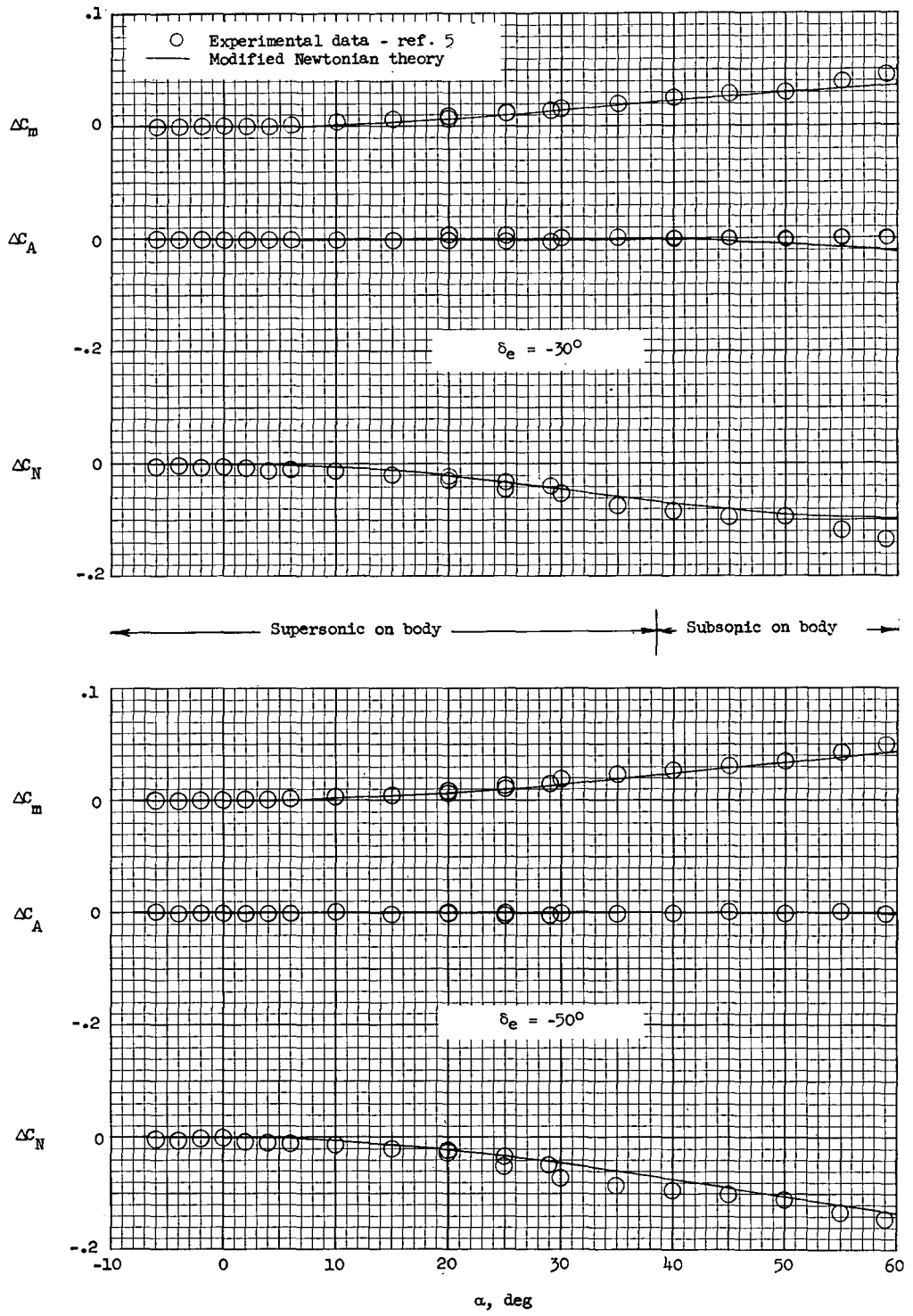

Figure 6.- Comparison of experimental longitudinal control effectiveness with modified Newtonian predictions for S_e/S_p = 0.1.

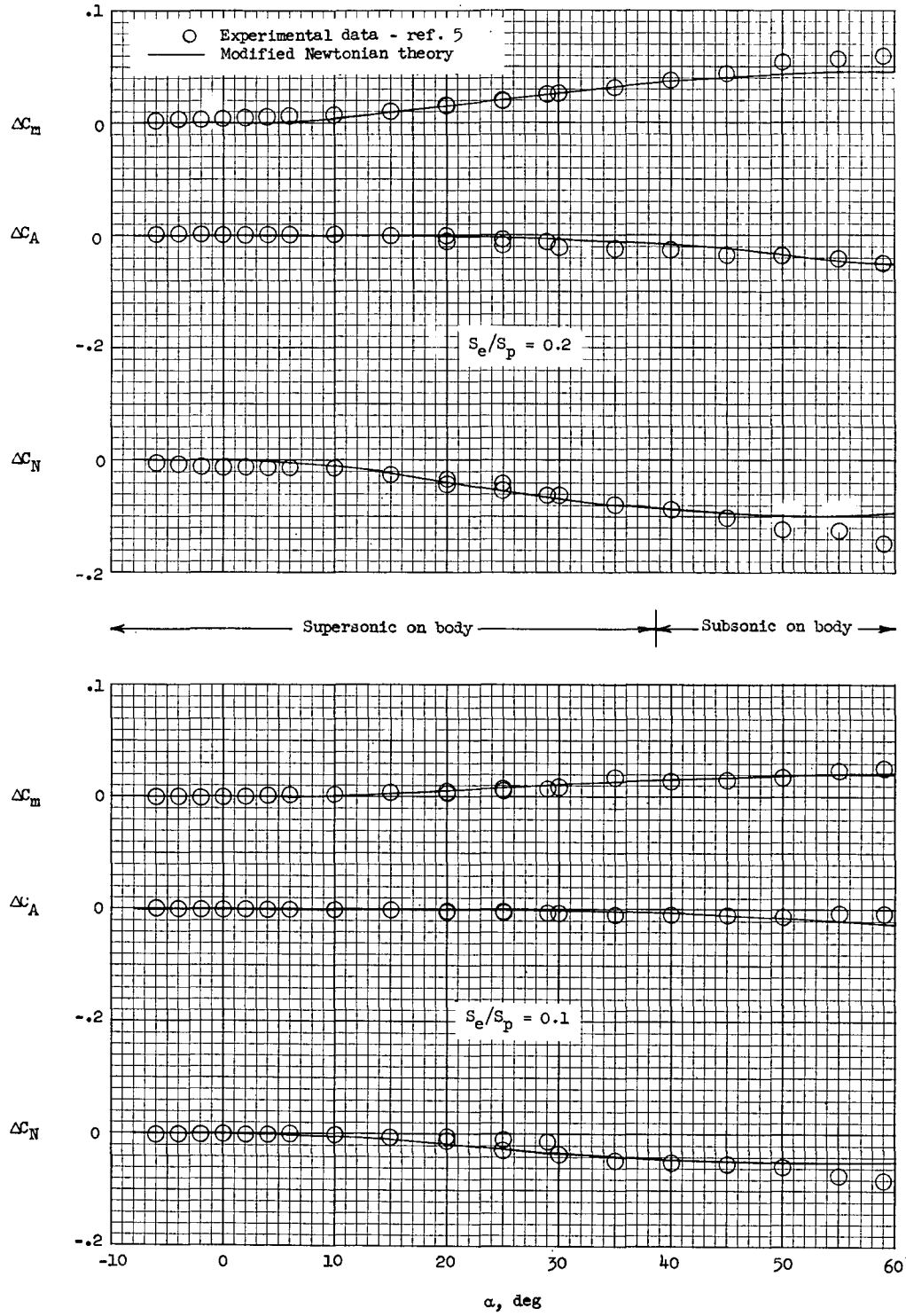

Figure 7.- Comparison of experimental longitudinal control effectiveness with modified Newtonian predictions for $\delta_e = -15^\circ$.

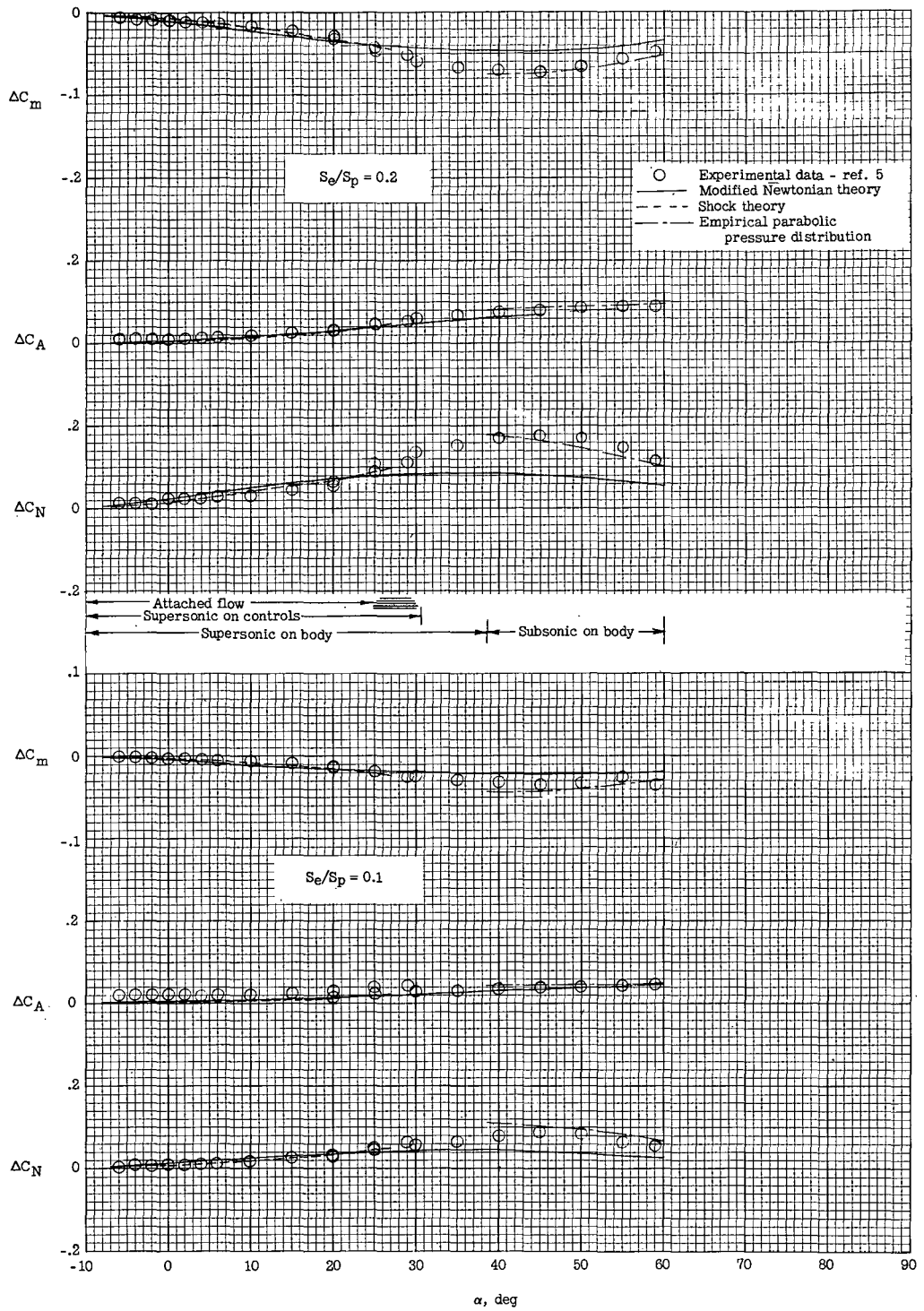

Figure 8.- Comparison of experimental longitudinal control effectiveness with modified Newtonian and shock theory for $\delta_e = 15^\circ$.

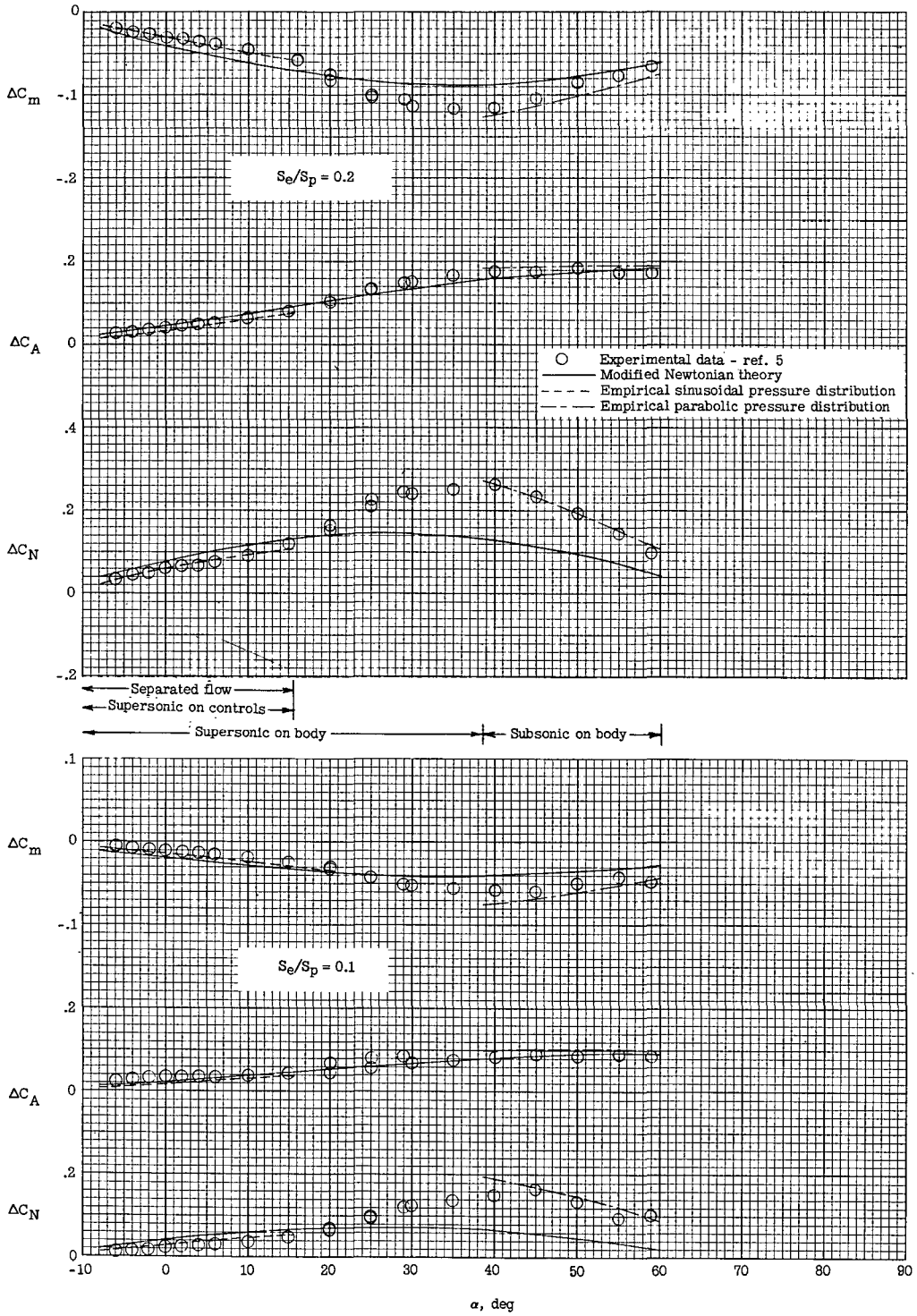

Figure 9.- Comparison of experimental longitudinal control effectiveness with predictions based on several theories for $\delta_e = 30^o$.

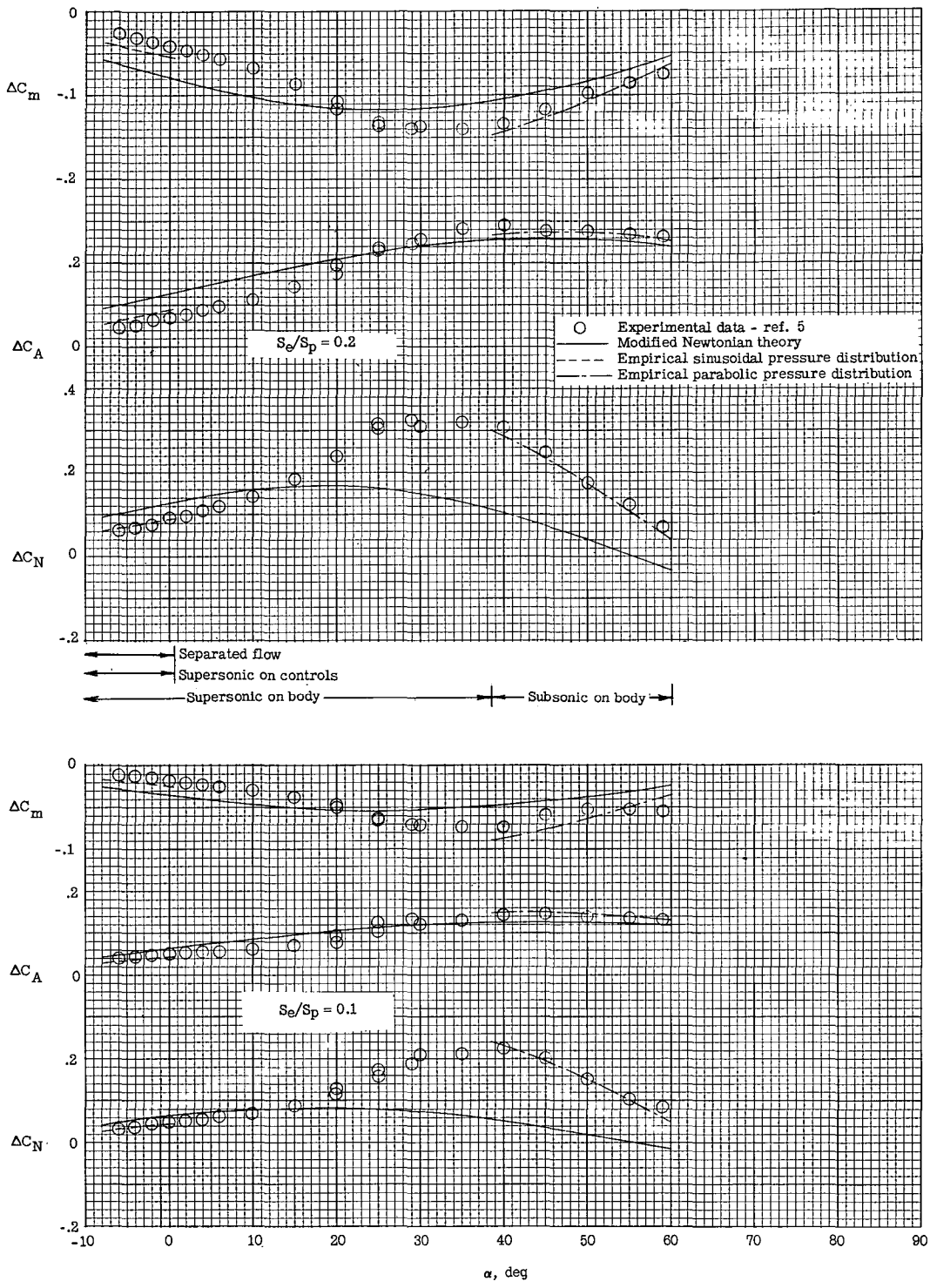

Figure 10.- Comparison of experimental longitudinal control effectiveness with predictions based on several theories for $\delta_e = 45^\circ$.

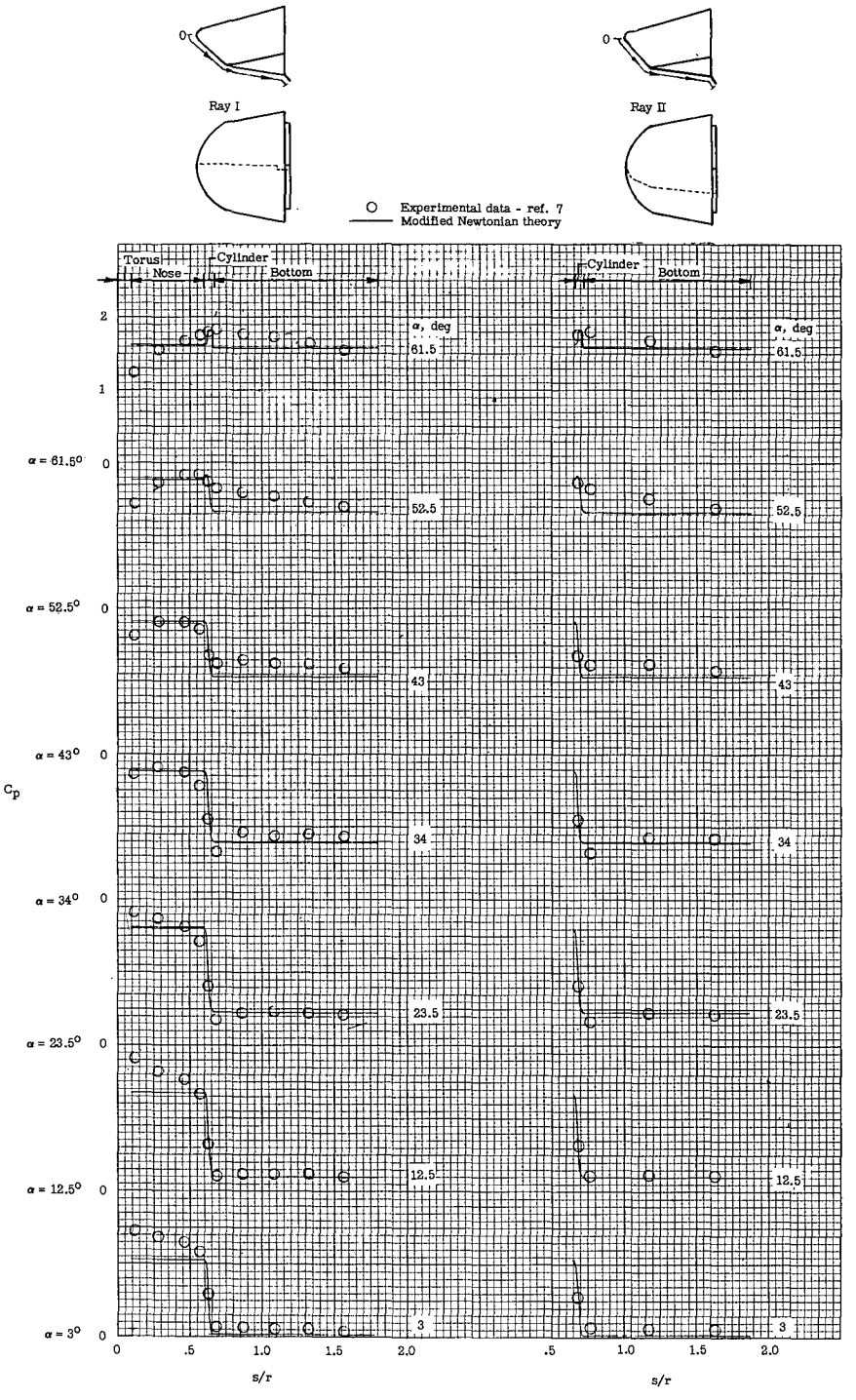

(a) Without aerodynamic controls.

Figure 11.- Pressure distribution along rays I and II.

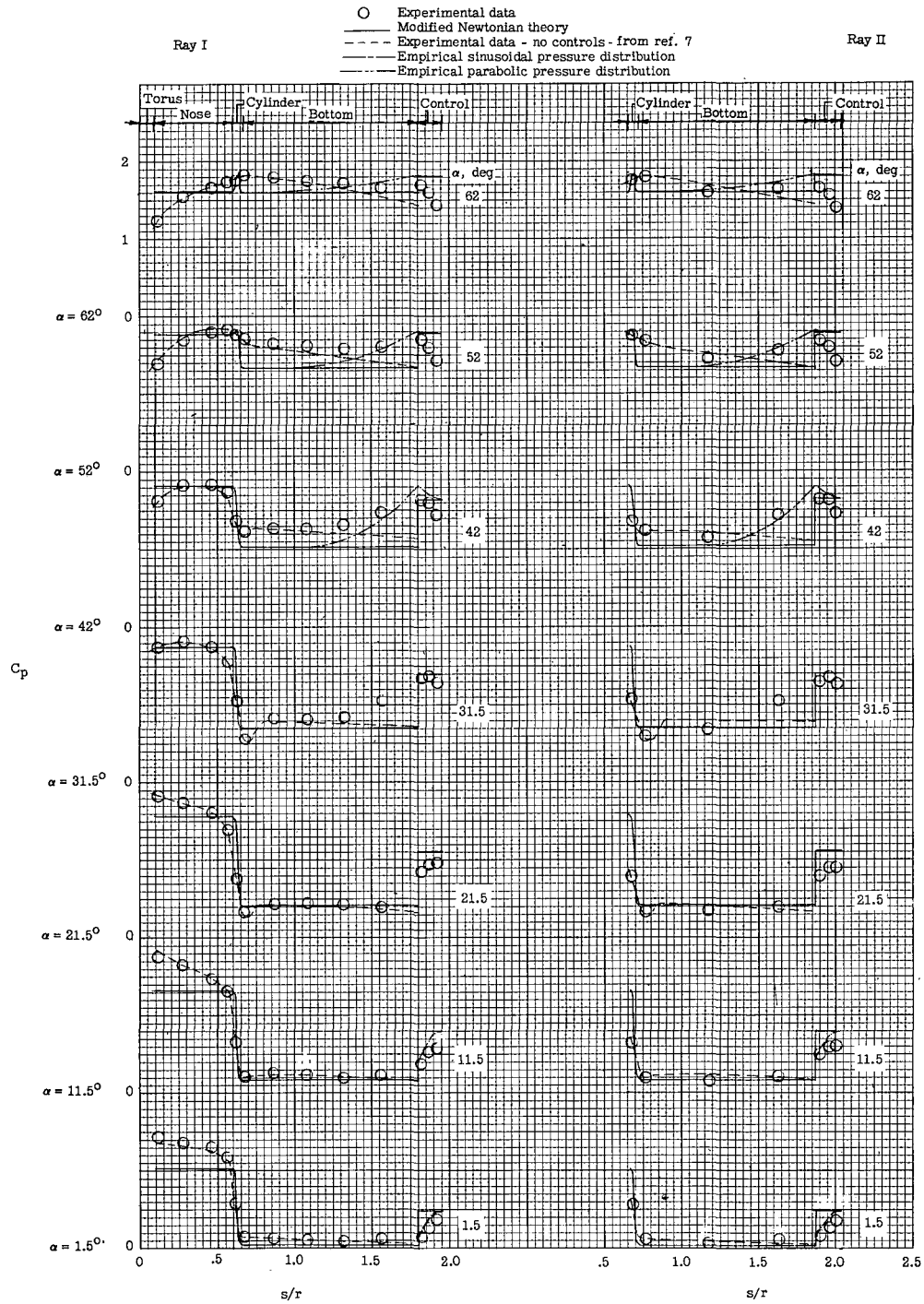

(b) $\delta_e = 30°$; $S_e/S_p = 0.1$.

Figure 11.- Continued.

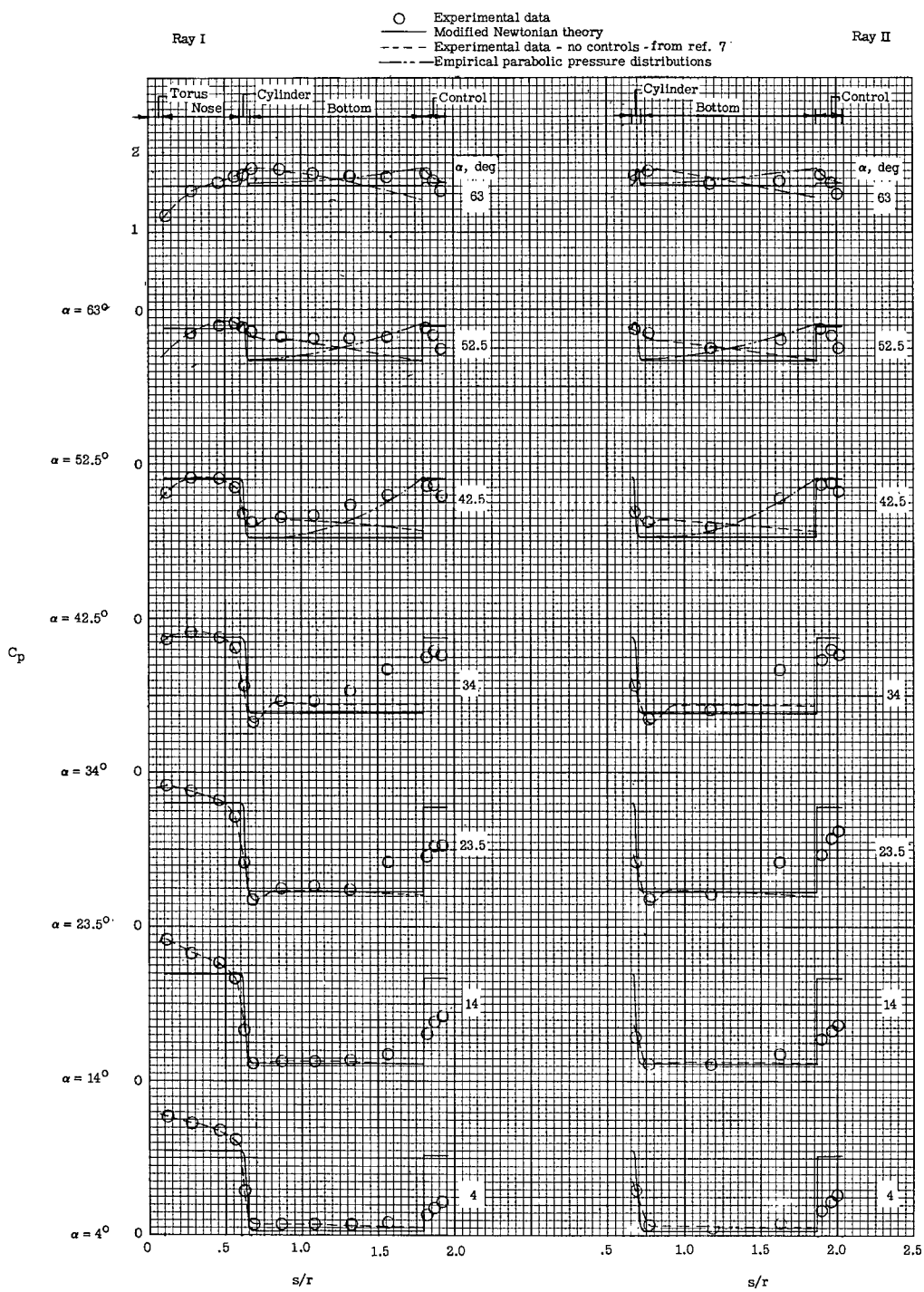

(c) $\delta_e = 45°$; $S_e/S_p = 0.1$.

Figure 11.- Continued.

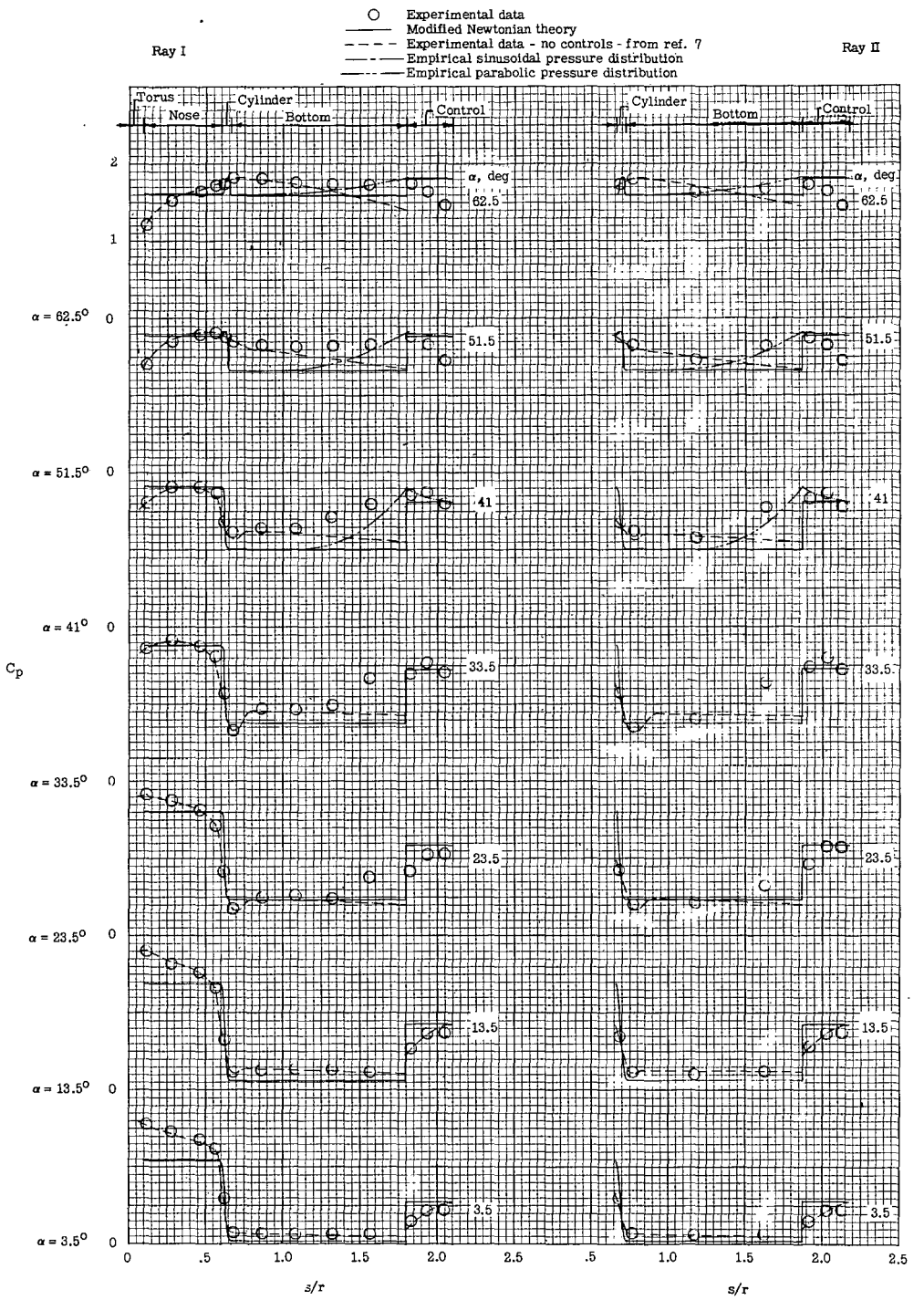

(d) $\delta_e = 30^\circ$; $S_e/S_p = 0.2$.

Figure 11.- Continued.

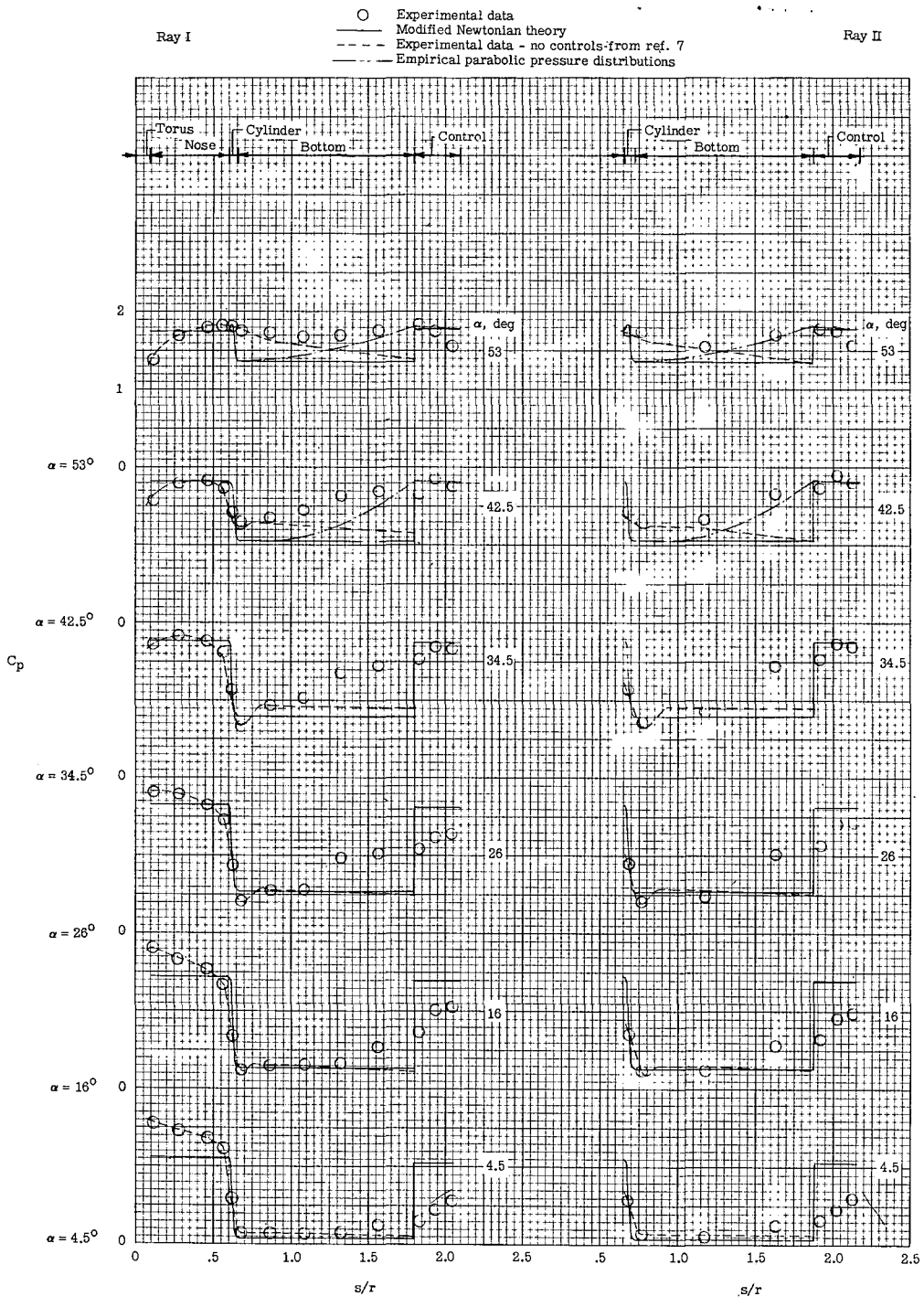

(e) $\delta_e = 45°$; $S_e/S_p = 0.2$.

Figure 11.- Concluded.

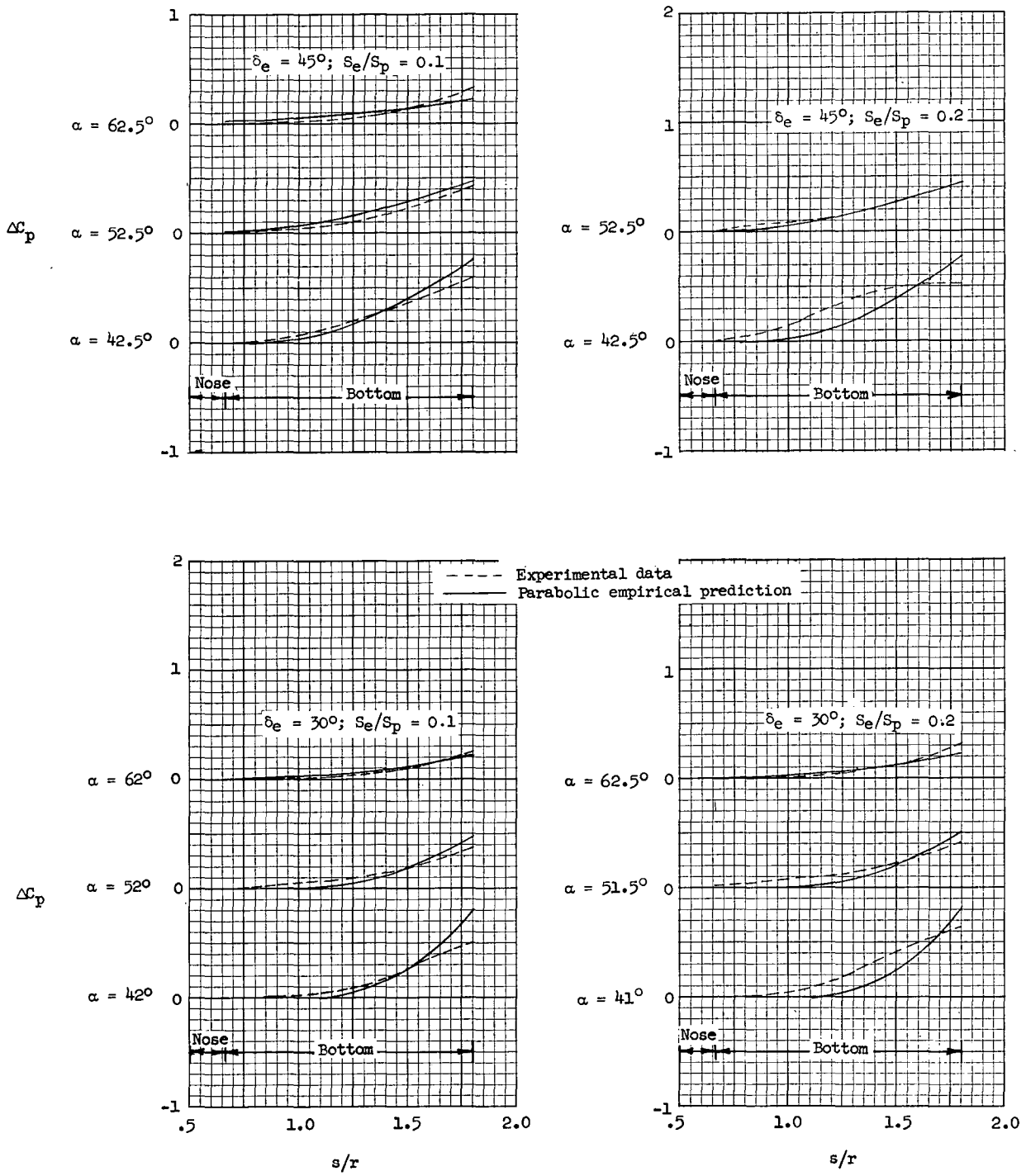

Figure 12.- Comparison of change in C_p due to addition of elevons (measured experimentally) with prediction of increase in C_p over Newtonian theory given by empirical parabolic pressure distribution (on center line of the bottom surface).

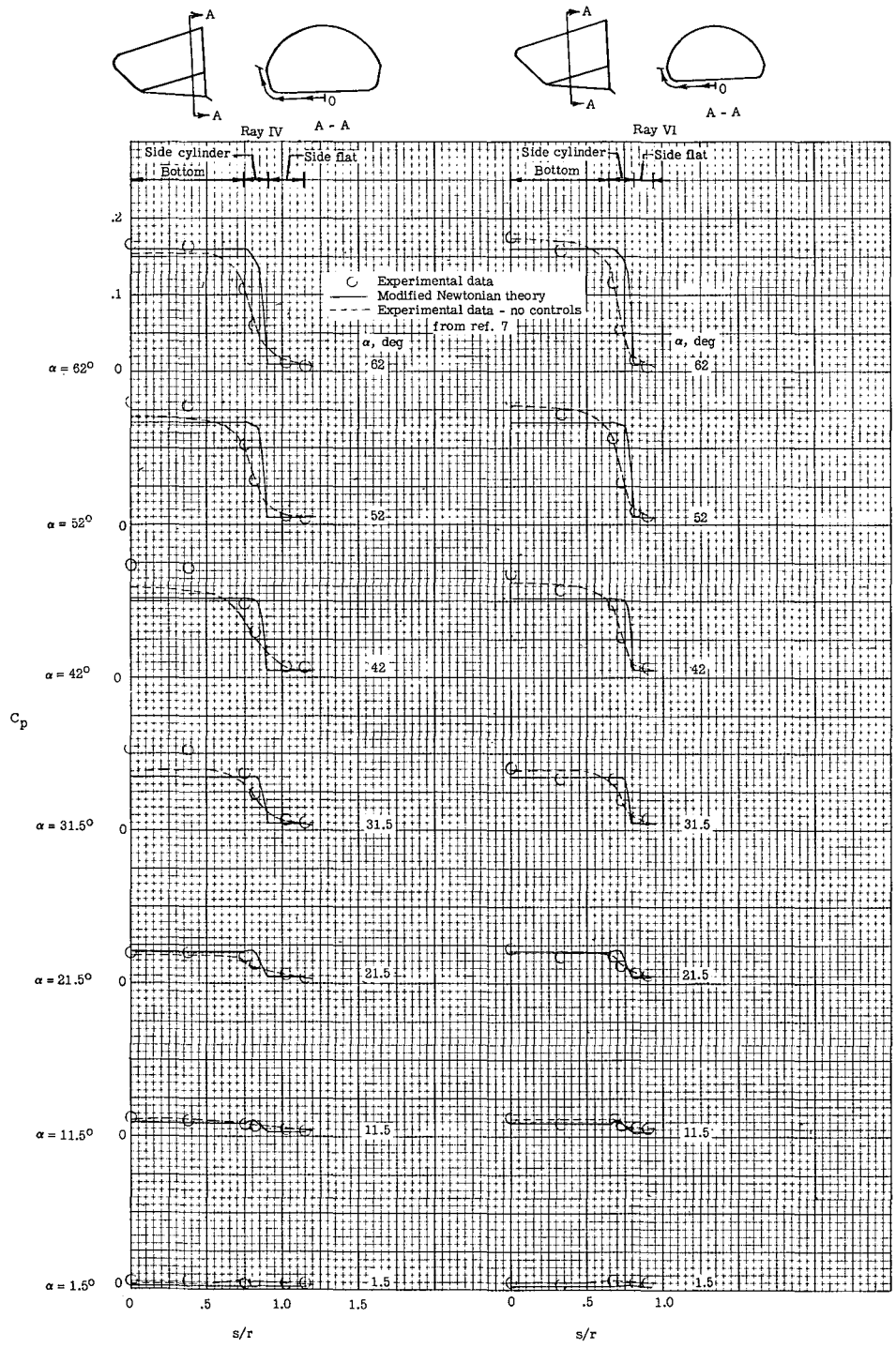

(a) $\delta_e = 30°$; $S_e/S_p = 0.1$.

Figure 13.- Pressure distribution along rays IV and VI.

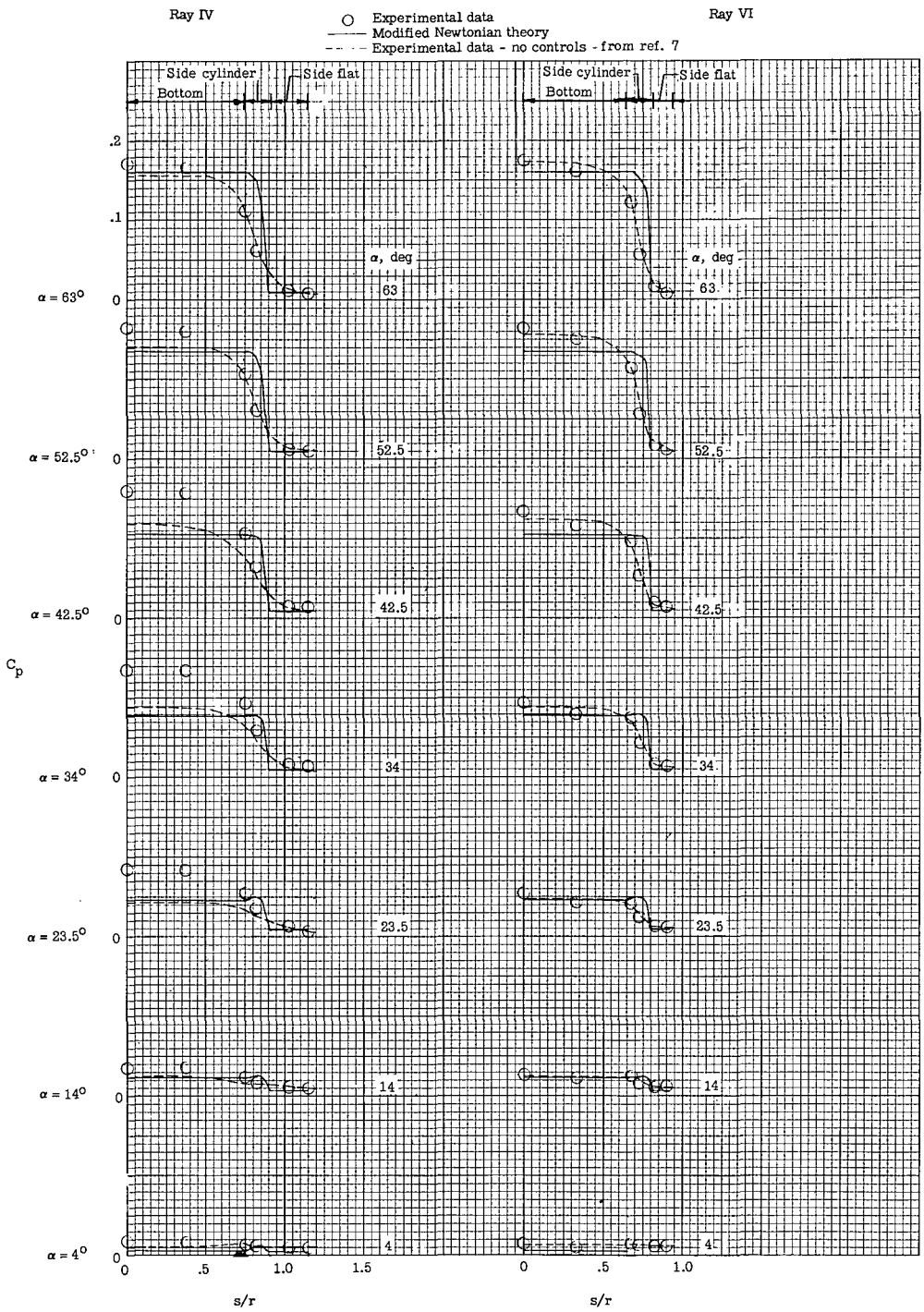

(b) $\delta_e = 45°$; $S_e/S_p = 0.1$.

Figure 13.- Continued.

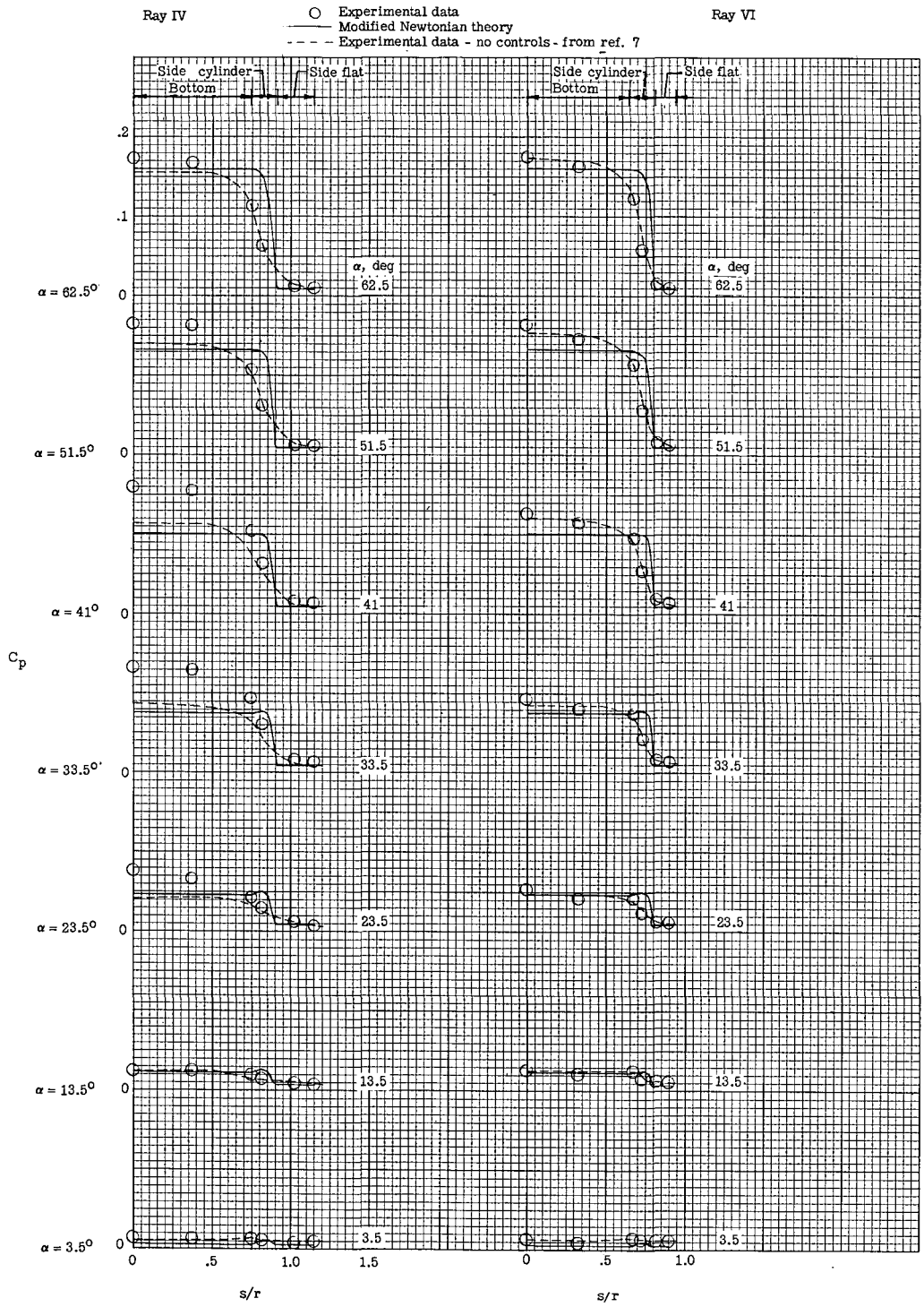

(c) $\delta_e = 30°$; $S_e/S_p = 0.2$.

Figure 13.- Continued.

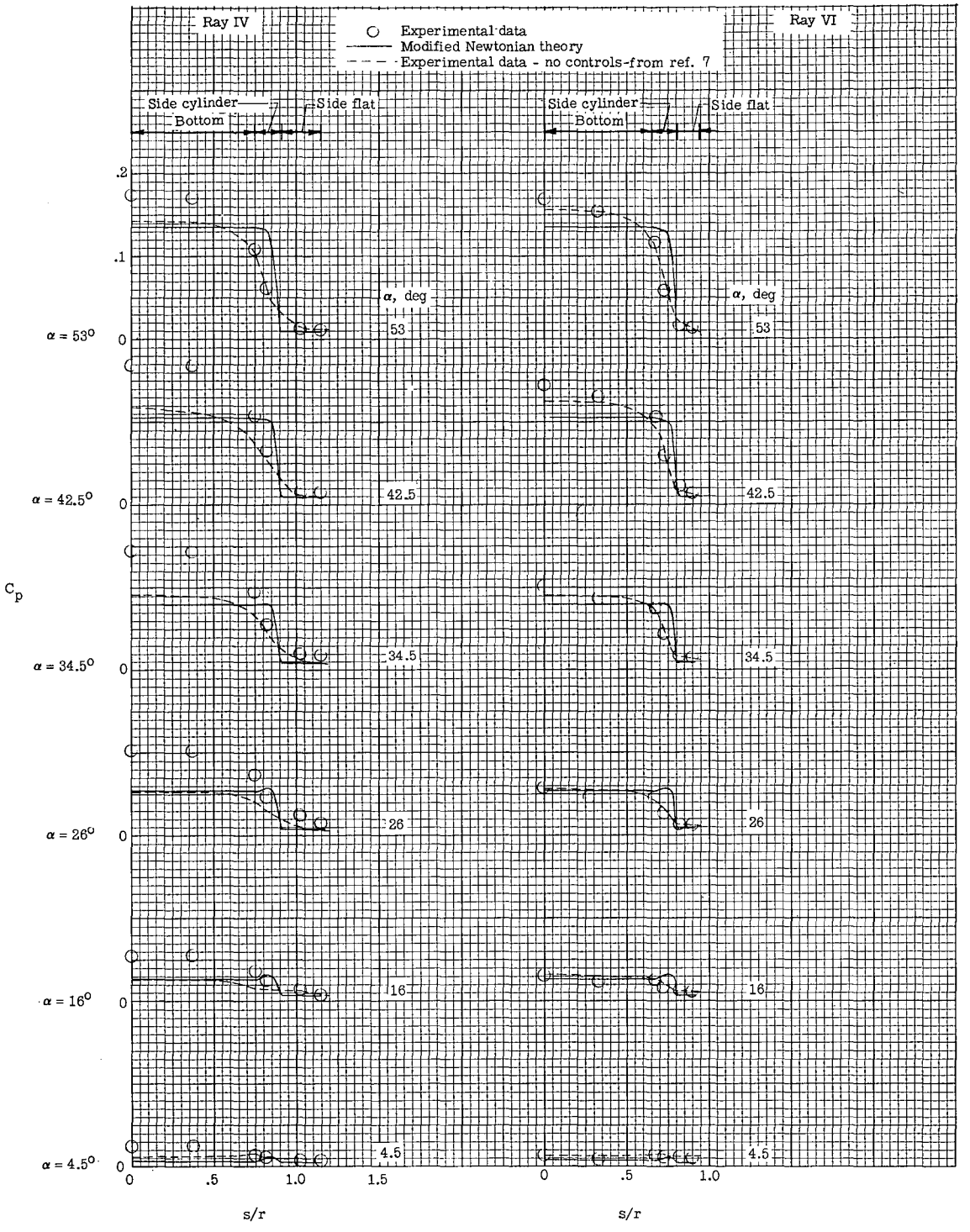

(d) $\delta_e = 45°$; $S_e/S_p = 0.2$.

Figure 13.- Concluded.

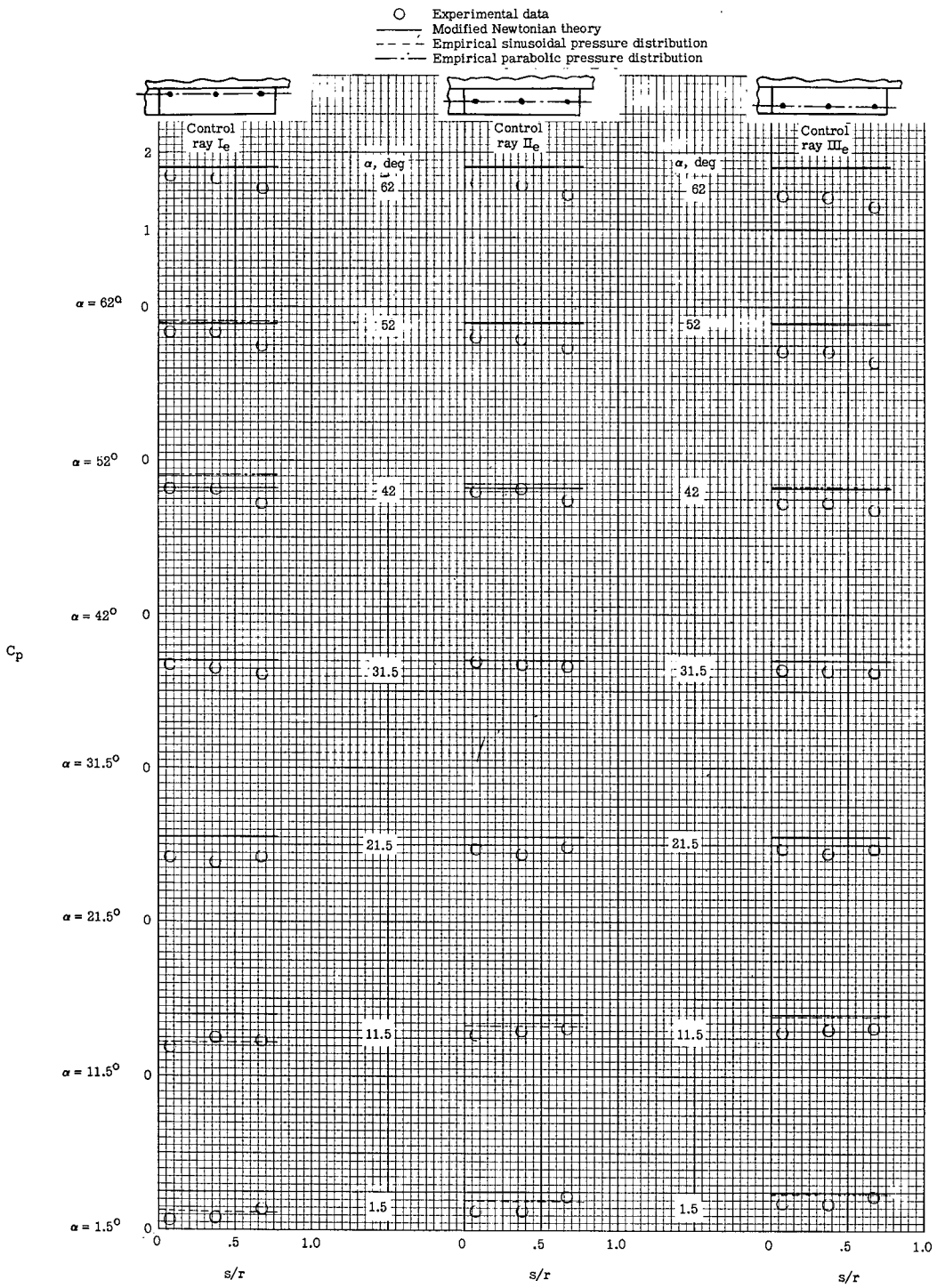

(a) $\delta_e = 30^\circ$; $S_e/S_p = 0.1$.

Figure 14.- Pressure distribution along control rays I_e, II_e, and III_e.

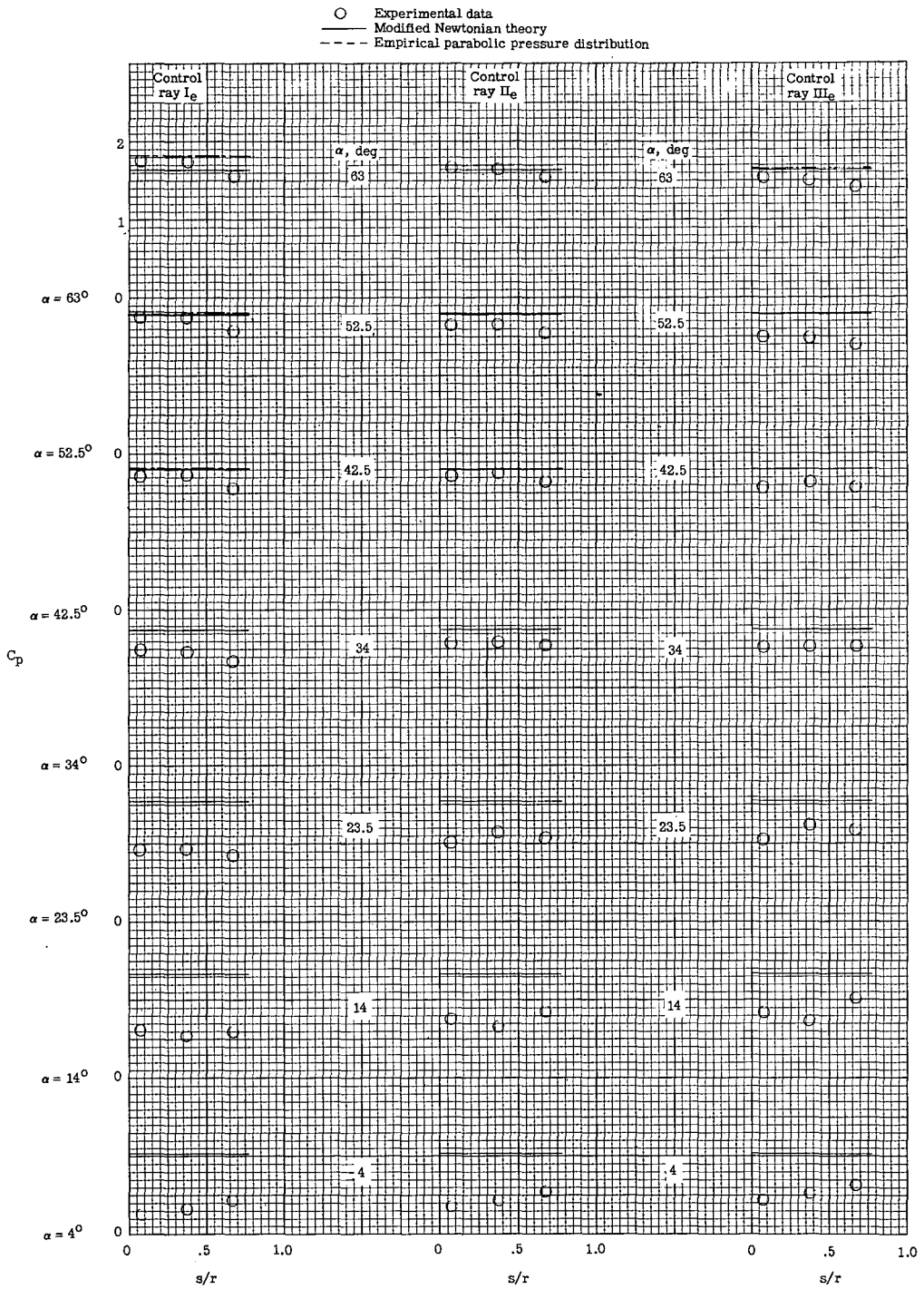

(b) $\delta_e = 45^\circ$; $S_e/S_p = 0.1$.

Figure 14.- Continued.

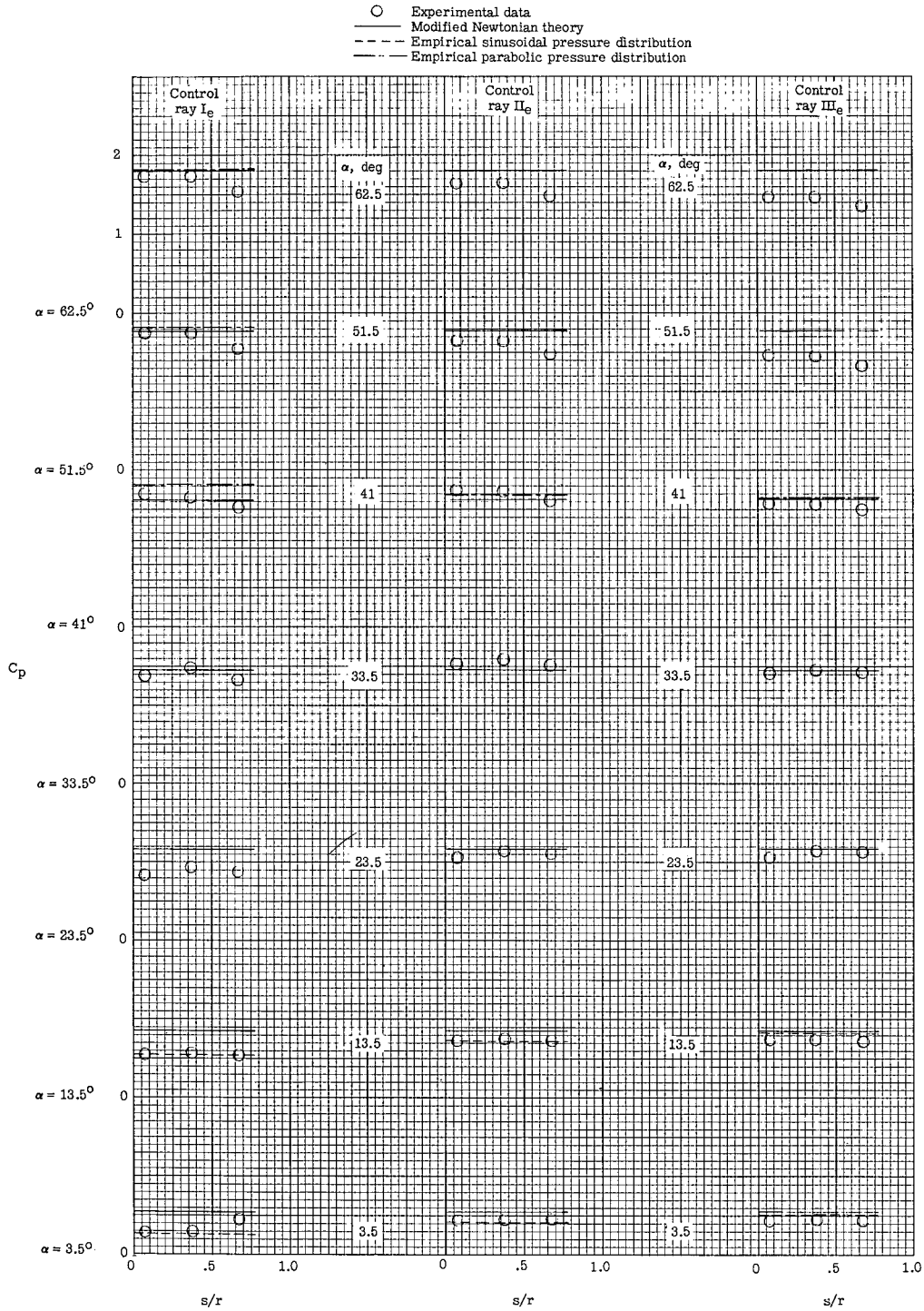

(c) $\delta_e = 30°$; $S_e/S_p = 0.2$.

Figure 14.- Continued.

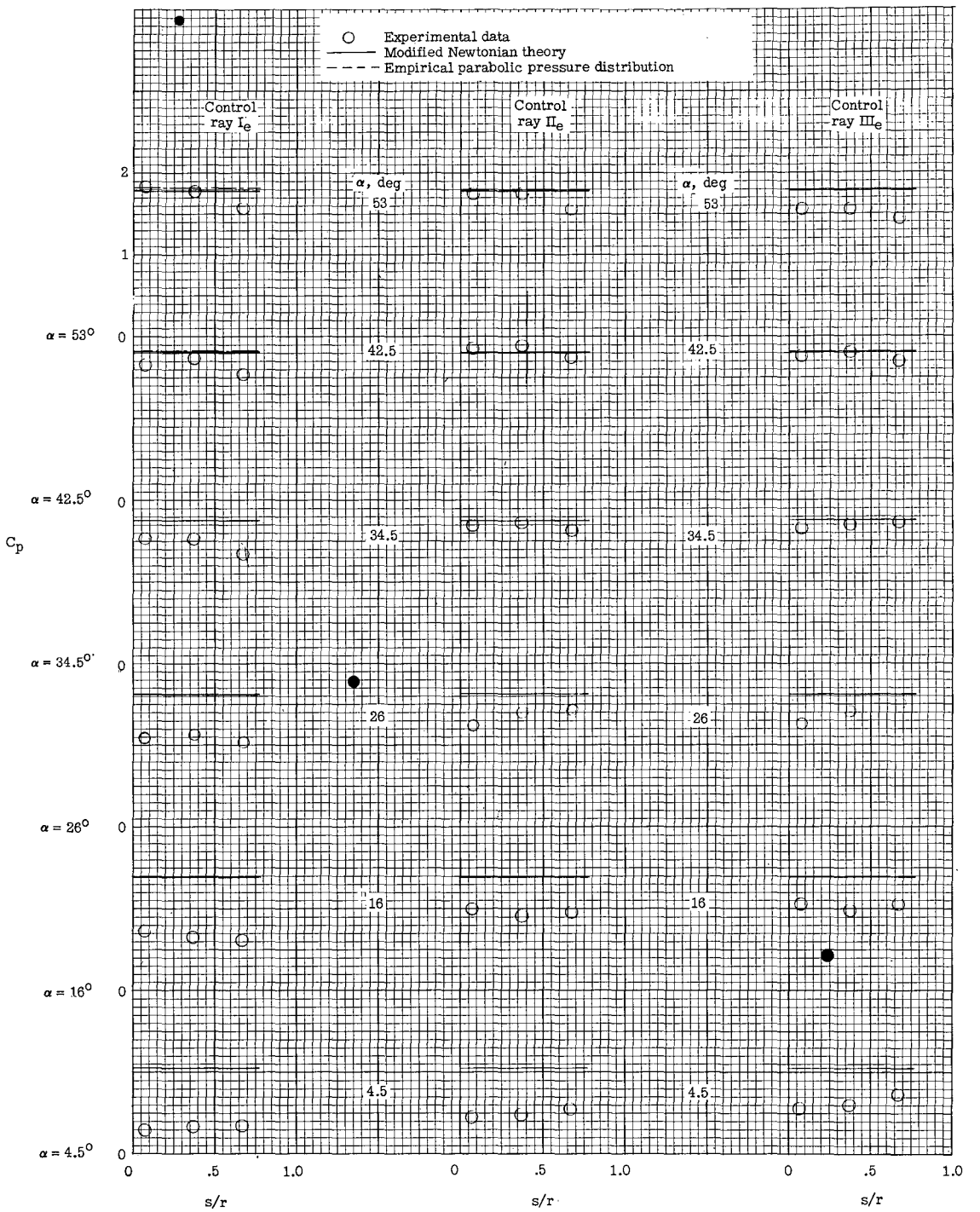

(d) $\delta_e = 45°$; $S_e/S_p = 0.2$.

Figure 14.- Concluded.

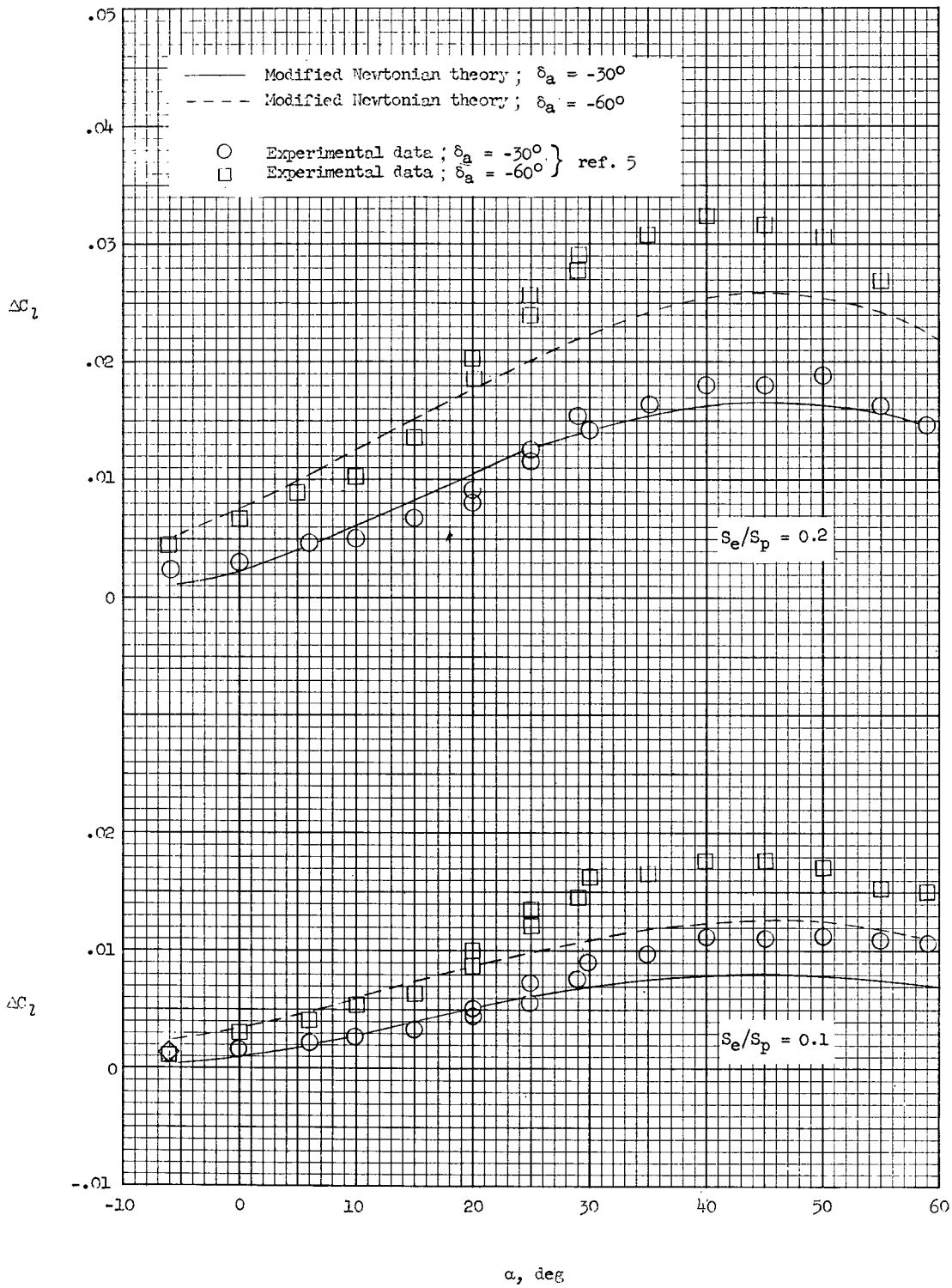

Figure 15.- Elevon effectiveness in roll control as compared with modified Newtonian predictions.

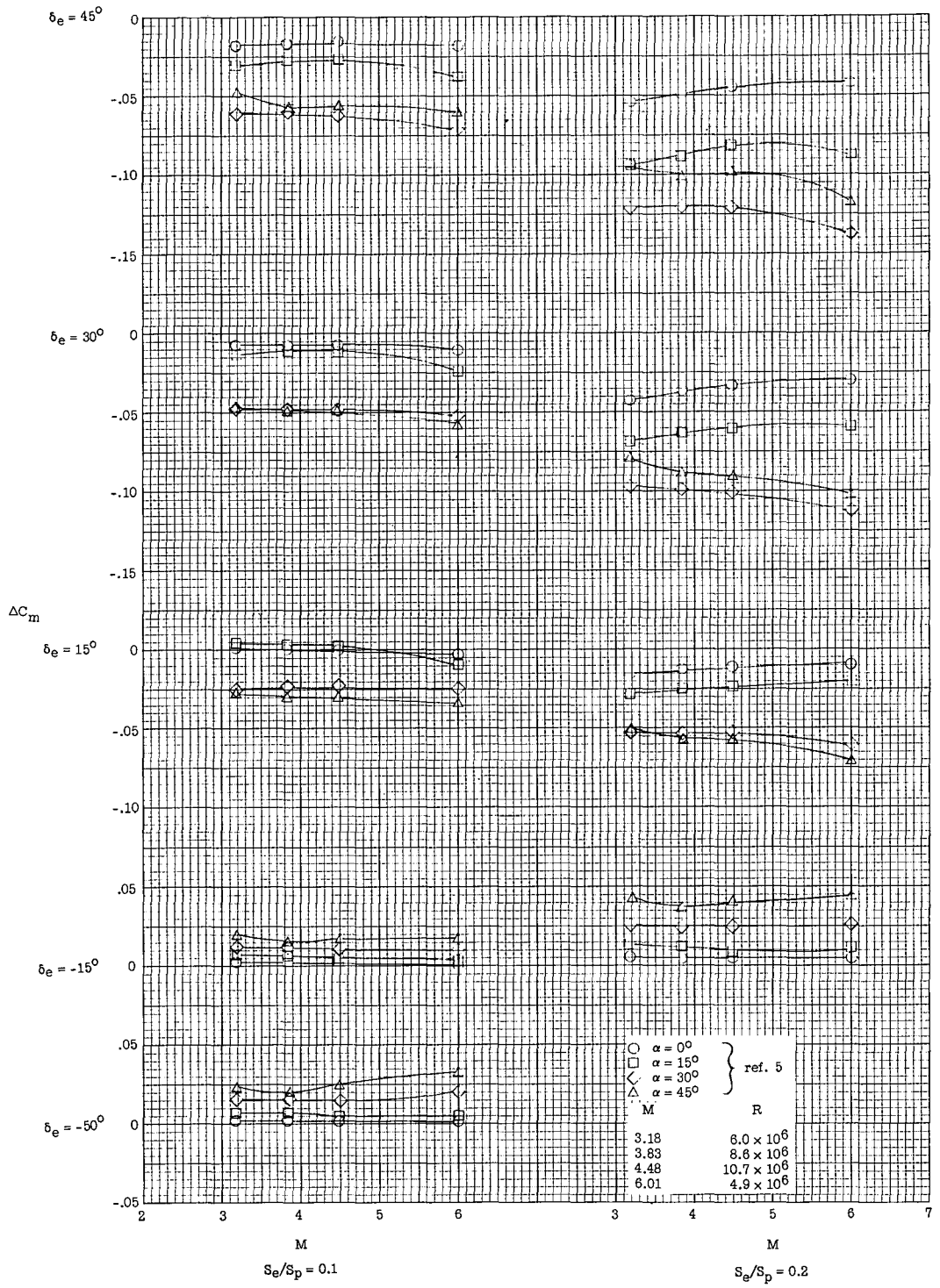

Figure 16.- Mach number effects on control effectiveness for a Reynolds number range of 4.9×10^6 to 10.7×10^6.